

1 **A detailed life history of a Pleistocene steppe bison (*Bison***
2 ***priscus*) skeleton unearthed in Arctic Alaska**

3
4 Juliette Funck^{1,2*}, Peter D. Heintzman^{3,4}, Gemma G. R. Murray⁵, Beth Shapiro^{3,6}, Holly
5 McKinney⁷, Jean-Bernard Huchet⁸, Nancy Bigelow⁹, Pat Druckenmiller^{2,10}, Matthew J.
6 Wooller^{1,11*}

7
8 1. Alaska Stable Isotope Facility, Water and Environmental Research Center, Institute of
9 Northern Engineering, University of Alaska Fairbanks, Fairbanks, AK 99775, USA.

10 2. Department of Geosciences, University of Alaska Fairbanks, Fairbanks, AK 99775, USA.

11 3. Department of Ecology and Evolutionary Biology, University of California Santa Cruz, Santa
12 Cruz, CA 95064, USA.

13 4. The Arctic University Museum of Norway, UiT - The Arctic University of Norway, NO-9037
14 Tromsø, Norway.

15 5. Department of Veterinary Medicine, University of Cambridge, Cambridge, CB3 0ES, UK.

16 6. Howard Hughes Medical Institute, University of California Santa Cruz, Santa Cruz, CA
17 95064, USA.

18 7. Department of Anthropology, University of Alaska Fairbanks, Fairbanks, AK 99775, USA.

19 8. Muséum National d'Histoire Naturelle, Institut de Systématique, Evolution, Biodiversité
20 (ISYEB), Unit Mixte de Recherche 7205, CP50, Entomologie, 45, rue Buffon, F-75005 Paris,
21 France.

22 9. Alaska Quaternary Center, University of Alaska Fairbanks, Fairbanks, AK 99775, USA

23 10. University of Alaska Museum of the North, Fairbanks, University of Alaska Fairbanks, AK
24 99775, USA.

25 11. College of Fisheries and Ocean Sciences, University of Alaska Fairbanks, Fairbanks, AK
26 99775, USA.

27

28 * Corresponding author e-mails: jmfunck@alaska.edu and mjwooller@alaska.edu

29

30 **Key words: Steppe Bison, Paleoecology, Isotopes, ancient DNA, Taphonomy**

31 **Abstract:**

32

33 Detailed paleoecological evidence from Arctic Alaska's past megafauna can help reconstruct
34 paleoenvironmental conditions and can illustrate ecological adaptation to varying environments.
35 We examined a rare, largely articulated and almost complete skeleton of a steppe bison (*Bison*
36 *priscus*) recently unearthed in Northern Alaska. We used a multi-proxy paleoecological approach
37 to reconstruct the past ecology of an individual representing a key ancient taxon. Radiocarbon
38 dating of horn keratin revealed that the specimen has a finite radiocarbon age ~46,000 +/- 1000
39 cal yr BP, very close to the limit of radiocarbon dating. We also employed Bayesian age
40 modeling of the mitochondrial genome, which estimated an age of ~33,000-87,000 cal yr BP.
41 Our taphonomic investigations show that the bison was scavenged post-mortem and infested by
42 blowflies before burial. Stable carbon and oxygen isotope ($\delta^{13}\text{C}$ and $\delta^{15}\text{N}$) analyses of
43 sequentially sampled horn keratin reveal a seasonal cycle; furthermore, high $\delta^{15}\text{N}$ values during
44 its first few years of life are consistent with patterns observed in modern bison that undertook
45 dispersal. We compared sequential analyses of tooth enamel for strontium isotope ratios
46 ($^{87}\text{Sr}/^{86}\text{Sr}$) to a spatial model of $^{87}\text{Sr}/^{86}\text{Sr}$ ratios providing evidence for dispersal across the
47 landscape. Synthesis of the paleoecological findings indicates the specimen lived during
48 interstadial conditions. Our multi-proxy, paleoecological approach, combining light and heavy
49 isotope ratios along with genetic information, adds to the broader understanding of ancient bison
50 ecology during the Late Pleistocene, indicating that ancient bison adopted different degrees of
51 paleo-mobility according to the prevailing paleoecological conditions and climate.

52

53 **Keywords:**

54 Quaternary; Beringia, Paleoecology; Stable Isotopes; Strontium; Oxygen; Carbon; Nitrogen;
55 Steppe Bison

56 **1. Introduction:**

57

58 ***1.1 Paleoeological context:***

59

60 Northern Alaska is currently experiencing environmental changes as the result of global
61 warming, which is occurring most rapidly at northern latitudes (Moon et al., 2019). These
62 changes impact the mobility and ecologies of extant megafauna including caribou, moose, and
63 muskoxen (Post and Forchhammer, 2008; Sharma et al., 2009). For example, migratory species
64 are experiencing mismatch in timing of migration and peak resource availability (Post and
65 Forchhammer, 2008), while caribou are losing habitat in the north due to warmer Arctic
66 summers and winters (Sharma et al., 2009). Detailed paleoecological evidence from the remains
67 of past megafauna from this region provides an opportunity to examine how past megafauna
68 lived in this environment (Guthrie, 1989), and therefore help predict responses of living
69 megafauna to present and projected environmental changes.

70 During the height of the last glaciation (~28-18 thousand years ago (kya)) (Clark et al.,
71 2009), the North Slope of Alaska was part of an expansive land-mass known as Beringia. Sea
72 levels were ~130 meters lower than today (Lambeck et al., 2014), exposing a shallow continental
73 shelf between northeast Asia and North America known as the Bering Land Bridge (BLB). The
74 BLB extended approximately from the Lena River, Russia, in the west and the Mackenzie River,
75 Yukon, Canada, in the east (Elias and Crocker 2008) (Figure 1). The Beringian ecosystem was
76 primarily that of a mammoth steppe, a graminoid-dominated ecosystem that supported a
77 community of large herbivorous mammals, dominated by mammoths (*Mamamuthus*
78 *primigenius*), horses (*Equus* sp.), and steppe bison (*Bison priscus*) (Guthrie, 2001; Mann et al.,
79 2013; Shapiro and Cooper, 2003; Zimov et al., 2012). The mammoth steppe supported large
80 populations of these herbivores, many of which had larger body sizes than their descendants
81 today at similar latitudes (Zimov et al., 2012). Bison, in particular, had larger body sizes and
82 horns than present-day American bison (*Bison bison*) (Martin et al., 2018), and were present
83 throughout most of Eurasia and North America in what has been termed “The Bison Belt”
84 (Guthrie, 1989). Steppe bison first arrived in North America ~195-135 kya (Froese et al., 2017)
85 and their population began to decline around 37 kya (Heintzman et al., 2016; Shapiro et al.,
86 2004).

87 Modern bison ecology can provide an analog for inferring ancient bison behavior as well
88 as the basis for comparative (paleo) biology and anatomy. Although modern plains bison (*Bison*
89 *bison bison*) are often considered grassland grazing specialists (Bamforth, 1987), plains bison in
90 northern habitats (Waggoner and Hinkes, 1986), wood bison (*Bison bison athabascae*) (Larter
91 and Gates, 1991), european wisents (*Bison bonasus*) have been observed to regularly utilize
92 browse in their diet (Kowalczyk et al., 2011). Evidence from macro and micro tooth-wear
93 analysis indicates that steppe bison likely had a broader herbivorous diet and ecological niche
94 that included browsing (Rivals et al., 2010, 2007; Saarinen et al., 2016). The long-distance
95 (>100km) (Berger, 2004; Hanson, 2015; Plumb et al., 2009) migrations of American bison
96 (*Bison bison*) across the American Great Plains were legendary and a key component of bison
97 life history (Bamforth, 1987; Flores, 1991). However, isotopic (strontium) analyses of ancient
98 (~18,500 ¹⁴C yr BP) bison (*Bison priscus*) from a site in Ukraine found no evidence of
99 paleomobility (Julien et al., 2012). Analyses of ancient bison specimens can provide
100 opportunities to flesh out the paleoecological life-history of a taxon that shaped Beringian
101 ecosystems (Zimov et al., 2011).

102 Fortunately for paleoecologists, bones, teeth, and horns of bison are some of the most
103 numerous fossil remains found in Alaska (Guthrie, 1970; Mann et al., 2013). On rare occasions,
104 high sediment deposition rates along with freezing temperatures can result in preservation of
105 virtually complete carcasses or skeletons of past Beringian fauna, revealing vivid paleoecological
106 snap-shots of life in Beringia (Boeskorov et al., 2016; Kirillova et al., 2015; Van Geel et al.,
107 2014; Zazula et al., 2017; Zazula et al., 2009). These rare and well-preserved glimpses of past
108 megafaunal paleoecology can emerge from eroding river-banks (Mann et al., 2013; Zazula et al.,
109 2009), during mining operations (Guthrie, 1968), and during construction activities (Zazula et
110 al., 2017). In some instances, soft tissue such as hair, skin, organs, and stomach contents are
111 preserved (Kirillova et al., 2015; Van Geel et al., 2014), as well as associated insects. These
112 remains, along with bones and teeth, can retain chemical clues about an individual's
113 paleoecology. Isotopic analyses (Kirillova et al., 2015) and analyses of ancient DNA (aDNA)
114 (Zazula et al., 2017) can reveal past mobility patterns and population interconnectivity,
115 contributing to an understanding of past ecosystems, landscapes, and evolution (Froese et al.,
116 2017; Haile et al., 2009; Marsolier-Kergoat et al., 2015; Shapiro and Cooper, 2003, Heintzman et
117 al., 2016; Shapiro et al., 2004).

118 In this study, we conducted a multi-proxy study, combining isotopic and aDNA analyses,
119 with supporting paleo-forensic analyses, to investigate the sex, age, paleoecology and life history
120 of an exceptionally well-preserved and largely articulated steppe bison (*Bison priscus*) found on
121 the North Slope of Alaska (Figure 1 a-c). We assess peri- and post-mortem events together with
122 the taphonomic history of skeletal remains using a taphonomic analysis of the skeleton and of the
123 plant and insect remains present. Our examination of the physical condition of the remains
124 (bones and teeth) from the specimen provides clues about an individual's age, sex, and
125 appearance (Fuller, 1959). The taphonomy and geology associated with the specimen provides
126 information about the context surrounding an organism's death and a possible cause of death.
127 We used insect (Elias et al., 2000) and plant (Bigelow et al., 2013) macrofossils associated with
128 the bison's remains to provide valuable paleoecological information. Our multi-proxy,
129 paleoecological approach adds to the broader understanding of ancient bison ecology during the
130 Late Pleistocene.

131

132 ***1.2 Stable Isotopes:***

133

134 Isotopic analyses have become a popular tool in paleoecology for determining the ecological and
135 life-history traits of ancient fauna (Bocherens, 2003; Britton et al., 2009). Tissues that form in
136 discrete layers over a period of an individual's life, such as tooth enamel, hair, or horn, can be
137 subsampled to allow inference of inter- and intra-annual paleo-mobility and paleoecology using
138 isotopic analyses of these sample types (Balasse et al., 2001; Britton et al., 2009; Stevens et al.,
139 2011; Zazzo et al., 2012). Intra-tooth strontium isotope ratio ($^{87}\text{Sr}/^{86}\text{Sr}$) analysis has been
140 developed as a useful tool to track the mobility of past animals and humans (Balasse, 2002;
141 Britton, 2009; Britton et al., 2011; Hoppe et al., 1999; Hoppe, 2004; Julien et al., 2012; Koch et
142 al., 1995; Pellegrini et al., 2008; Radloff et al., 2010; Viner et al., 2010; Widga et al., 2010).
143 $^{87}\text{Sr}/^{86}\text{Sr}$ ratios can vary across landscapes depending in part on the age and rock type of the
144 underlying geology (Bataille et al., 2014; Brennan et al., 2014). These landscape $^{87}\text{Sr}/^{86}\text{Sr}$
145 signatures can enter animals through their diet and drinking water, replacing calcium in tissues
146 such as teeth and bones (Capo et al., 1998). The combination of $^{87}\text{Sr}/^{86}\text{Sr}$ ratios and oxygen
147 isotopic ($\delta^{18}\text{O}$) values from analyses of animal tissues have proved to be a powerful predictor of
148 geographic location (Britton et al., 2009; Gignoux et al., 2017; Knudson et al., 2009). The $\delta^{18}\text{O}$

149 values from a specimen can indicate location based on latitude and distance from the coast
150 (Hoppe, 2006; Lachniet et al., 2016). The $\delta^{18}\text{O}$ values from analyses of bison teeth have also
151 been used to determine approximate local climate and seasonal temperature variation, because
152 $\delta^{18}\text{O}$ values in water can be closely related to temperature (Bernard et al., 2009; Hoppe et al.,
153 2006; Scherler et al., 2014). Examining bison mobility has been one of the more common
154 applications of this isotopic methodology, partly due to the abundance of bison remains in the
155 archaeological and paleontological records (Britton et al., 2012; Julien et al., 2012; Widga et al.,
156 2010).

157 Stable carbon and nitrogen isotope ratios (expressed as $\delta^{13}\text{C}$ and $\delta^{15}\text{N}$ values,
158 respectively) from analyses of sub-fossils of animals can add a dietary dimension to a
159 paleoecological reconstruction (Drucker et al., 2008; Stevens and Hedges, 2004). $\delta^{13}\text{C}$, along
160 with $\delta^{18}\text{O}$, values can be generated from the analysis of inorganic carbon in bones and teeth
161 (Koch et al., 1997). Bison horns, which grow throughout the life of a bison, are a carbon and
162 nitrogen-rich keratin tissue that allows intra- and inter-annual paleoecological inferences. $\delta^{13}\text{C}$
163 values can also be generated from analyses of organic carbon preserved as bone collagen and the
164 horn keratin, these methods also produce $\delta^{15}\text{N}$ values (Iacumin et al., 2001; Schoeninger and
165 DeNiro, 1984). In order to interpret the $\delta^{13}\text{C}$ and $\delta^{15}\text{N}$ values of these analyses, potential sources
166 of variability need to be evaluated. One common source of $\delta^{13}\text{C}$ variation in the diet of
167 herbivores is variation in the proportional contribution C_4 vs. C_3 plants. However, C_4 plants are
168 exceedingly rare or non-existent in the Arctic (Wooller et al., 2007). Furthermore, a lack of trees
169 and even shrubs in Pleistocene Arctic Alaska, even during some warmer interglacials (Willerslev
170 et al., 2014), also excludes “the canopy effect” caused by the concentration of CO_2 in dense
171 forest (Drucker et al., 2008) and differences between herbs and shrubs (Schwartz-Narbonne et
172 al., 2019). Thus, the main source of variability in $\delta^{13}\text{C}$ values we can expect in Arctic vegetation
173 is between wetter and drier environments (Wooller et al., 2007).

174 There are several drivers of $\delta^{15}\text{N}$ variation in animals, which can make it a challenging
175 system to study although $\delta^{15}\text{N}$ values can demonstrate important relationships. For example,
176 $\delta^{15}\text{N}$ values in ancient megafauna have been found to have a strong relationship with the amount
177 of precipitation during the Pleistocene (Carlson et al., 2016; Drucker et al., 2003; Graham et al.,
178 2016; Heaton et al., 1986; Rabanus-Wallace et al., 2017), which is likely due in part to major
179 changes in soil ecology in response to climatic change (Hobbie and Hobbie, 2006; Stevens et al.,

2006). However, for higher resolution $\delta^{15}\text{N}$ we must consider behavioral and physiological explanations for change found in serially analyzed tissues (Drucker et al., 2010). Behavioral explanations including migration or dispersal could explain some of the differences and $\delta^{15}\text{N}$ values found in relation to aridity (Barbosa et al., 2009) and altitude (Männel et al., 2007). In northern regions, studies have found consistent difference in plants based on mycorrhizal relationships with the soil (Kristensen et al., 2011). However, these are not sufficient to account for the seasonal differences or major regional differences that would be required to explain some of the magnitude of variation in $\delta^{15}\text{N}$ values we go on to document in this ancient bison and other modern bison in the region (Funck et al., 2020). Alternatively, physiological changes in $\delta^{15}\text{N}$ values of animals can occur in animals adapted to extreme conditions. Notably, animals who undergo hibernation (Lee et al., 2012), lack sufficient calories or are fasting (Hobson et al., 1993; Hobson and Clark, 1992; Mekota et al., 2006; Voigt and Matt, 2004) as well as animals managing acute physical stress (Delgiudice et al., 2000; Fuller et al., 2005; Habran et al., 2010; Rode et al., 2016) can exhibit relatively large increases in $\delta^{15}\text{N}$ values. The effect of dietary stress on $\delta^{15}\text{N}$ values in wood bison was evident in individuals that had undergone nutritional stress during the winter in Northern Alaska (Funck et al., 2020). For this reason, we will focus our interpretation on nutritional stress as the primary factor of intra-tissue $\delta^{15}\text{N}$ variation but acknowledge that other behavioral and ecological factors may be involved. From our review of the literature, we have noted that changes in $\delta^{15}\text{N}$ values in herbivores from the mammoth steppe over time have largely not included the possibility that some of the variation could be driven by physiological stress and even starvation. To some degree this is likely obscured by the fact that a majority of the previous research has focused on $\delta^{15}\text{N}$ values generated from analyses of bone collagen, which provides a more integrated and essentially a life-time measure. Our analyses of horn-sheaths are providing a new a more detailed temporal perspective, which could be translated to the huge abundance of archived bison horn sheaths available. Using a combination of isotopic approaches on different sequentially grown tissues can provide a multi-proxy perspective of an individual's life-history and eventually put this in the context of larger herds.

207

208 ***1.3 Ancient DNA:***

209

210 Ancient DNA (aDNA) from ancient bison specimens from Beringia has been used to monitor
211 gene-flow across the BLB and through the ice-free corridor that connected eastern Beringia to
212 the rest of the Americas (Froese et al., 2017; Heintzman et al., 2016). It has also been used to
213 estimate past changes in effective population size (Lorenzen et al., 2011), which has been used to
214 identify the decline of steppe bison since ~37 kya in Beringia (Shapiro et al., 2004). Analyses
215 using aDNA can also add a further perspective on individual steppe bison specimens. They can
216 provide information on an individual's genomic sex and population affinity, and help constrain
217 age estimates for specimens potentially outside the range or towards the limits of radiocarbon
218 dating. For the latter analysis, one such approach uses Bayesian analysis of aDNA sequences
219 from dated specimens that lived at different time periods to calibrate a molecular clock, and then
220 use this calibration to estimate the age of the undatable individual (Shapiro et al., 2011). The
221 mitochondrial genealogy of Pleistocene bison in North America has been relatively well
222 sampled, both geographically and temporally (Froese et al., 2017; Heintzman et al., 2016;
223 Shapiro et al., 2004), and is therefore likely to be well suited for estimating the age of ancient
224 bison specimens.

225

226 **2. Material and methods:**

227

228 ***2.1 Specimen and study site:***

229

230 Dr. Dan Mann and Dr. Pamela Grooves found a nearly complete, and partially articulated
231 specimen of steppe bison (*Bison priscus*) eroding out of a bank of the Ikpikpuk River on the
232 North Slope of Alaska (Figure 1 a-c) located at 69.71563 N, -154.863 W (WGS 84) (Figure 1).
233 They excavated and transported to the University of Alaska Museum of the North (UAMN),
234 where the University of Alaska Museum Earth Sciences collections (UAMES) assigned an
235 identification number UAMES 29458. The North Slope of Alaska is delimited by the Brooks
236 Range of mountains to the south and the Arctic Ocean to the north (Figure 1). The southern
237 portion is predominantly low foothills that become a coastal plain at ~69° north. The Ikpikpuk
238 River cuts through Quaternary-aged aeolian sand deposits, known as the Ikpikpuk Sand Sea
239 (Carter, 1981). These deposits preserve an abundance of Quaternary vertebrate fossils that erode
240 from banks of the Ikpikpuk River, though rarely in such excellent and complete condition (Mann

241 et al., 2015). The general geology of this region consists of undifferentiated alluvial and aeolian
242 deposits (organic-rich silt, loess and sand) of Holocene to Pleistocene age. The specimen was
243 discovered and excavated from the eroding banks of the Ikpikpuk River in these unconsolidated
244 sediments. The vast majority of vertebrate remains recovered from here are single isolated
245 elements found in reworked sediments while floating the river by small boat. Unfortunately, a
246 quarry map is not available from the site at the time of collection, in part due to the unexpected
247 nature of the find and constraints of rapidly conducting fieldwork in remote Alaska. The
248 sediment and associated microfossils analyzed in this study were collected from matrix directly
249 surrounding or within cavities of the skeleton.

250

251 ***2.2 Fossil Material:***

252

253 Skeletal elements of specimen UAMES 29458 were removed from the encasing sediment,
254 cleaned, and anatomically re-articulated (Figure 2a). Hair, preserved soft tissue, and associated
255 sediment were stored by individual body element and kept frozen. We rearticulated the specimen
256 at the UAMES (Figure 2 a, b) and examined it for signs of scavenging and other taphonomic
257 processes, using methods outlined elsewhere (Binford, 1981; Domínguez-Rodrigo, 1999; Fisher,
258 1995; Haynes, 1980; Hudson, 1993; Lyman, 1994, 1987). We found a large number of
259 invertebrate and plant macrofossils within the interstices of the skull, particularly the brain
260 cavity. These were collected and identified to provide taphonomic and paleoenvironmental
261 context. We removed larger macrofossils and examined them using a dissecting microscope. We
262 wet sieved sediments at 150 μm and 250 μm . All diagnostic plant macrofossils were collected
263 from sediments larger than 250 μm and all invertebrate materials were collected and archived.

264

265 ***2.3 Radiocarbon analysis:***

266

267 Radiocarbon dating was conducted on different materials associated with specimen UAMES
268 29458. Previously the bone collagen from the cap of a spinous process, extracted without
269 ultrafiltration, was analyzed at Beta Analytic (Miami, Florida), and found to be non-finite in age
270 $>43,500$ radiocarbon years (Mann et al., 2013). However, collagen is porous and can be subject
271 to contamination, so we selected additional materials for further analysis: keratin from the horn

272 sheath, along with a fly pupal case and a plant macrofossil (herbaceous stem) that were both
273 recovered from inside the bison skull. W. M. Keck Carbon Cycle Accelerator Mass Spectrometry
274 Laboratory analyzed the samples on a National Electrostatics Corporation (NEC 0.5MV
275 1.5SDH-2 AMS system). The horn sheath keratin was run alongside three non-finite-¹⁴C aged
276 bison horn sheath samples and the mean blank from these three was subtracted from sample
277 results, with an assumed 30% uncertainty. All of the sample preparation backgrounds were also
278 subtracted, based on measurements of a ¹⁴C-free wood standard, with an assumed 30%
279 uncertainty.

280

281 **2.4 Isotopic analyses:**

282

283 We removed thirty-three intra-tooth subsamples of enamel from the right mandibular molars 1,
284 2, and 3 (M1, M2, M3) of UAMES 29458 (Supplemental Figure 1). We collected samples in a
285 laminar flow hood at the Alaska Stable Isotope Facility (ASIF) at the University of Alaska
286 Fairbanks (UAF). We removed the surface layer of the target region from each molar and
287 subsequently used a Dremel diamond-coated circular saw to divide samples along each tooth
288 parallel to the growth plane (Figure S1). Enamel samples were removed as chips, which has been
289 found to reduce the potential for contamination (Diego Fernandez, University of Utah, ICPMS
290 Facility 2018 personal communication).

291 The University of Utah, Department of Geology and Geophysics, ICPMS facility
292 analyzed half of each sample for ⁸⁷Sr/⁸⁶Sr ratios using a multi-collector inductively coupled
293 plasma mass spectrometer (MC-ICPMS - ThermoFisher Scientific, High Resolution NEPTUNE,
294 Bremen, Germany). Strontium isotope analyses followed previously published protocols
295 (Glassburn et al., 2018; Nelson et al., 2018). Additionally, we sampled **whole** molars from 14
296 modern rodent museum specimens (UAM:Mamm: *Microtus oeconomus*, *Microtus mirus*,
297 *Dicrostonyx groenlandicus*) from within a 250-km radius surrounding the UAMES 29458
298 locality (Figure 1a) to determine the bioavailable ⁸⁷Sr/⁸⁶Sr ratios in the region (Bataille et al.,
299 2020). This method has previously been used to determine local bioavailable ⁸⁷Sr/⁸⁶Sr ratios for
300 comparison to mobile individuals (Hoppe et al., 1999; Kootker et al., 2016; Radloff et al., 2010).
301 The results of this investigation augment existing spatial models of variability in ⁸⁷Sr/⁸⁶Sr ratios
302 in Alaska (Bataille et al., 2014).

303 We chemically pre-treated the remaining half of each bison enamel sample to remove
304 contaminants from gas exchange using the modified method from Pellegrini and Snoeck (2016,
305 2015) in order to produce $\delta^{18}\text{O}$ and $\delta^{13}\text{C}$ values. To compensate for the use of small ($\sim 1 \times 2$ mm)
306 enamel chips rather than powder we increased the soaking time. We added one milliliter of 2%
307 sodium hypochlorite (NaOCl) to each sample, shaken to mix, and soaked for 48 hours to remove
308 organic particulates. We then rinsed samples with deionized water and soaked them in 1 M
309 acetate buffered acetic acid (0.1 M) ($\text{CH}_3\text{CO}_2\text{H}$) for 48 hours to removed carbonate portion.
310 Finally, we rinsed the samples three times with deionized water before freezing and then freeze-
311 dried them for approximately 10 hours on a VirTiS benchtop Lyo-Centre lyophilizer to remove
312 any moisture prior to isotopic analysis. We analyzed the carbonate fraction using a Thermo
313 Scientific GasBench II carbonate analyzer attached to a Thermo Scientific DeltaV^{Plus} Isotope
314 Ratio Mass Spectrometer at ASIF following previously published protocols (Glassburn et al.,
315 2018). Stable carbon and oxygen isotope ratios are reported in δ notation as parts per thousand
316 (‰) relative to the international standard Vienna Pee Dee Belemnite (VPDB). We ran the
317 samples with laboratory standards of calcium carbonate (Merck, Suprapur 99.95% Lot #
318 B510959 313) every 10 samples to determine analytical precision for $\delta^{13}\text{C}$ values (0.3 ‰) and
319 $\delta^{18}\text{O}$ values (0.2 ‰) (all errors are expressed as one standard deviations). The $\delta^{18}\text{O}$ and $\delta^{13}\text{C}$
320 values were initially determined relative to VPDB for oxygen and carbon, but the $\delta^{18}\text{O}$ values
321 were subsequently converted to the Vienna Standard Mean Ocean Water (VSMOW) scale to
322 allow comparison of the values to meteoric water values. The $\delta^{18}\text{O}$ values were converted to
323 VSMOW using Formula 1 (below) (Verkouteren and Klinedinst, 2004) and then Formula 2
324 (below), a conversion developed by Hoppe et al. (2006) and Velivetskaya et al. (2016) to
325 compare bison enamel to meteoric water $\delta^{18}\text{O}$ values:

326

327 Formula 1: $\text{VSMOW} = 30.92 + 1.03092 * \text{VPDB}$

328

329 Formula 2: $\text{Enamel carbonate} = 0.7(\pm 0.12) * \text{VSMOW} - 30.06(\pm 1.40)$

330

331 We removed horn sheath keratin as a wedge perpendicular to the direction of the keratin
332 growth layers (Figure S2). We selected the location to maximize the years of horn growth
333 covered by the core. We then subsampled the core by peeling off thin layers between 0.1-0.3 mm

334 in thickness with a razor blade, for a total of $n = 113$ sub-samples. Sub-samples were analyzed to
335 produce $\delta^{15}\text{N}$ and $\delta^{13}\text{C}$ values (vs. AIR for nitrogen and VPDB for carbon) using a Flash 2000
336 Organic Elemental Analyzer (EA) connected via a ConFlo IV to an IRMS (DeltaV Plus) at ASIF.
337 Internal reference checks using peptone (No. P-7750 meat-based protein. Sigma Chemical
338 Company, Lot #76f-0300) were run every 10th sample, and blanks were run every 20th sample.
339 Repeated measurements of standards provided the analytical precisions, which were ± 0.1 ‰ and
340 ± 0.6 ‰ for $\delta^{15}\text{N}$ and $\delta^{13}\text{C}$ values, respectively.

341

342 **2.5 aDNA analyses:**

343

344 The first premolar (PM1) of specimen UAMES 29458 was sent to the specialized Paleogenomics
345 Laboratory at the University of California Santa Cruz (UCSC) for aDNA analysis. We followed
346 standard protocols as outlined in Froese et al. (2017) to extract and analyze ancient DNA unless
347 stated otherwise. Briefly, we extracted aDNA using a silica column method (Dabney et al.,
348 2013), and then converted extracts into an Illumina-compatible double-stranded DNA library
349 (Meyer and Kircher, 2010). We enriched an aliquot of this DNA library for bison mitochondrial
350 genomic fragments using a commercial MyBaits target capture kit (Arbor Biosciences, Ann
351 Arbor, MI). We sequenced both the enriched and remaining unenriched library on separate runs
352 of an Illumina MiSeq using v3 150 cycle chemistry75 cyc, with paired-end 75 bp reads. We then
353 merged the paired-end read data, trimmed adapters, and removed short (<25 base pairs (bp) for
354 the enriched library; <30 bp for the unenriched library) and low-complexity sequences (DUST
355 cutoff: 7) using SeqPrep and PRINSEQ-lite v0.20.4 (Schmieder and Edwards, 2011).

356 We aligned the filtered reads from the unenriched library to a reference database that
357 included the cow (*Bos taurus*) genome (Genbank: Btau_4.6.1) and an American bison (*Bison*
358 *bison*) mitochondrial genome (Genbank: NC_012346), using the Burrows Wheeler Aligner
359 (BWA; Li and Durbin, 2009) aln algorithm with the seed disabled (-l 1024). We filtered aligned
360 reads by map quality score (minimum of 20) and removed duplicates using SAMtools v0.1.19
361 (Li and Durbin, 2009). We assessed aDNA damage patterns using mapDamage v2.0.9 (Jónsson
362 et al., 2013). To infer the genomic sex of UAMES 29458, we followed the method of Heintzman
363 et al. (2017), which compares the relative mapping frequency of the X chromosome to the

364 autosomes. A male is inferred if this ratio is 0.45-0.55, whereas the expectation for a female is
365 0.95-1.05.

366 We mapped the filtered reads from the enriched library to a steppe bison reference
367 mitochondrial genome (Genbank: KX269138) using the multiple iterative assembler (MIA;
368 Briggs et al. 2009) and BWA, as above. For aDNA damage assessment of the enriched data, we
369 used the BWA mapping consensus results as the reference sequence for mapDamage. We
370 calculated a mitochondrial genome consensus sequence from the MIA mapping results using the
371 criteria outlined in Froese et al. (2017), and added this sequence to the full mitochondrial
372 genome alignment of Froese et al. (2017), as modified by Zazula et al. (2017). This alignment
373 consisted of four yak and 47 Siberian or North American bison mitochondrial sequences.

374 Before estimating the age of UAMES 29458 with Bayesian time-tree methods, we tested
375 for temporal signal in the data set. Tip-dating methods are only valid if this signal is present, as
376 these methods will usually converge on an estimate whether or not there is a temporal signal
377 present (Firth et al., 2010). We used a linear regression of phylogenetic root-to-tip distance
378 against the sampling date to test for temporal signal (following Murray et al., 2016). We
379 estimated a neighbor-joining tree of the data set (excluding the yak and two radiocarbon non-
380 finite bison sequences) using a K80 nucleotide substitution model with pairwise deletion, using
381 the ape package in R (Paradis et al., 2004), in which the root was fit simultaneously with the
382 regression, so as to minimize the residual mean squares, with the resulting root matching the root
383 obtained by using the yak sequences as an outgroup. Analyses of the full alignment and a
384 reduced alignment, with MS022 omitted (see below), returned positive correlations that are
385 significantly different from random permutations over clusters of samples with similar dates
386 (full: $r = 0.50$, $p = 0.010$; reduced: $r = 0.44$, $p = 0.025$; Figure S3). We defined similar-date
387 clusters ($n=34-35$) as monophyletic clades that had the same date after rounding to the nearest
388 thousand years. A Mantel test suggested that this clustering was sufficient to eliminate a
389 correlation between genetic and temporal distances in the data (without clustering: $p = 0.001$,
390 with clustering: $p = 0.18$) (Murray et al., 2016), which can result in a false positive result.
391 Overall, these analyses suggest the presence of temporal signal in the bison mitochondrial
392 genome data set.

393 We then estimated a time-tree in BEAST (v1.10.4, Drummond et al., 2012) so as to
394 estimate both the age of UAMES 29458 and its placement in the bison mitochondrial genome

395 phylogeny. We used a strict molecular clock with either finite radiocarbon dates or stratigraphic
396 data associated with the other sequences in the analysis as priors, following Froese et al. (2017)
397 and Zazula et al. (2017). To estimate the age of UAMES 29458, we used a uniform prior
398 distribution of between 30 kya BP (as this specimen is borderline radiocarbon finite; see results)
399 and 195 kya BP (the earliest mitochondrial estimate for the arrival of bison in North America;
400 Froese et al., 2017), following the method of Shapiro et al. (2011). To test the robustness of the
401 oldest age estimates, we also ran analyses with the minimum age prior set at 0, 20, 40, or 50 kya
402 BP. We ran analyses with each set of priors twice, each time with the Markov chain Monte Carlo
403 (MCMC) chains run for 60 million iterations, sampling every 3,000 iterations, and discarding the
404 first 10% as burn-in. Using Tracer v1.6, we observed that all parameters reached convergence
405 with the exception of the tree likelihood, which swapped between two optima in all analyses.
406 This was due to the shifting placement of sequence MS022 (KX269130; Froese et al., 2017).
407 This sequence was therefore removed from the alignment and all analyses were re-run.
408 Convergence was then observed for all parameters. For each prior and alignment result set, we
409 summarized trees and calculated a maximum clade credibility tree. All ages are reported as 95%
410 highest posterior density (HPD) credibility intervals.

411

412 **3. Results:**

413

414 ***3.1 Physical description:***

415

416 Overall, we observed specimen UAMES 29458 to be relatively complete and well preserved
417 (Figure 2). Based on the observed number of annual growth cycles visible in the horn sheath, we
418 estimated the bison specimen to be minimally 12 years old, which is considered a mature
419 individual (Fuller, 1959). The specimen's horn span was 90 cm at the widest point and the
420 comparative angle and length of the horns indicate that it was a male (Guthrie, 1966). Much of
421 the hair had sloughed off the specimen and was found in the surrounding sediment. In some
422 areas, hair and skin had dried to the bone and were still attached. Hair from the front and hind
423 limbs was yellow ochre in color, as were the shorter undercoat hairs from the body. The longer
424 hairs were a reddish-brown or dark brown and tail hairs were black to dark brown. Long hairs

425 found in the surrounding sediment, which likely came from the cape (hair on the shoulders),
426 beard (long hair on the chin) or cap (long hair on the top of the head), were light to dark brown.

427 The skull was in excellent condition and the left and right mandibles were fused at the
428 symphysis. The incisors were missing from a pre-burial break. There were no gnaw marks on the
429 surrounding bone to indicate another animal had gnawed them off. Evidence of root etching was
430 observed on the ventral surfaces of the mandible with vivianite deposits observed on the articular
431 surface. Vivianite was identified visually, it is commonly found on fossils found in these
432 environments, and is unique in its blue appearance. We observed that the cervical vertebra 2 (C2)
433 through thoracic vertebra 7 (T7) had the dorsal portion of the spinous process gnawed (Figure
434 3b) and bitten off (Figure 3a). We also observed T4 and T5 had evidence of damage from a
435 carnivore, including puncture marks (Figure 3 a). Lumbar vertebra 1 (L1) to the sacrum also had
436 evidence of carnivore damage on the ventral surface of the vertebrae (Figure 3 b). The distal
437 ends of four thoracic ribs (towards the anterior portion of the body) also had puncture marks and
438 gnawing. There were several pre- and post-burial breaks, and several medial portions of the ribs
439 were missing. One rib on the right side had a pathology consistent with a healed break (Figure
440 3c). The left side was missing two thoracic ribs. The costal cartilage had carnivore gnawing
441 damage on two fragments and the manubrium was missing one section.

442 The right appendicular skeleton was complete and we observed no evidence of carnivore
443 damage. In addition, there was soft tissue (keratinous hoof sheathes, leather-like flesh and
444 connective tissue) and vivianite present. There were gnaw and puncture marks observed on the
445 proximal end of the left humerus (lateral tuberosity) near its articulation with the scapula; the
446 scapula was missing. There was root etching on the medial surface of the humerus where it
447 would have rested on the ground after the specimen's death and we observed soft tissue adhering
448 to the bone. The left metacarpal, carpals, and proximal, medial, and distal phalanges were
449 missing, which could be consistent with loss during taphonomic processes upon emerging from
450 the riverbank because the bones would have been exposed first and eroded out of the bank. In
451 addition to the lack of carnivore marks near the articulations, they do not possess much food
452 value for a carnivore and would not have been a primary target. On the left femur there was a
453 pre-burial break at the greater trochanter, but no obvious carnivore damage. The left patella,
454 calcaneus, several left tarsals, one sesamoid, one proximal, medial and distal phalanx was

455 missing, which is also consistent with secondary loss upon the specimen eroding out of the
456 riverbank.

457

458 **3.2 Radiocarbon analysis:**

459

460 We generated three new radiocarbon dates associated with specimen UAMES 29458 (Table 1).
461 The background-subtracted fraction modern values for both the keratin and insect chitin are
462 different from zero by ~6 standard deviations, which indicates the ages are finite. The age of the
463 keratin from the bison horn sheath was $46,000 \pm 1,100$ ^{14}C yr BP (46,962 cal yr BP using CALIB
464 7.1; (Stuiver et al., 2019)), which was very similar to the radiocarbon date produced from the
465 keratinous fly puparium (Table 1, Figure 4) taken from inside the bison skull cavity ($46,800 \pm$
466 $1,200$ ^{14}C yr BP, just outside the range for calibration using CALIB 7.1 (Stuiver et al., 2019). The
467 dated plant macrofossil found in the skull, along with the puparia, had a radiocarbon date of
468 $>49,900$ radiocarbon years, which was outside the range for calibration (Table 1).

469

470 **3.3 Macrofossils:**

471

472 **3.3.1 Fossil plant remains**

473

474 The contents of the neural canal of the spine and skull from specimen UAMES 29458 included a
475 sand-rich matrix with abundant moss, wood, and we could identify other plant fragments to
476 species in some instances (Figures 4 and 5). The plant macrofossil assemblage from inside the
477 skull is consistent with a mesic tundra or a wet flood plain surrounded by a shrub tundra (Figure
478 5). The presence of *Daphnia* spp. ephippia indicate that the sediment was also, at least partially,
479 aquatic in origin. Bryophytic material, likely from wet tundra and rivers, was abundant and well
480 preserved in the skull cavity. Wood was very common and possibly came from the shrubs
481 identified from seeds, leaves, and other materials in the skull cavity, including *Salix* spp.
482 (willow), *Betula* spp. (birch), and *Andromeda polifolia* (bog rosemary) (Figure 4 n). These
483 shrubs are typical of wet tundra and tend to be more abundant in more protected areas (Cody,
484 2000; Hulten, 1968), suggesting an interstadial environment. In addition, *Potentilla palustris* and
485 *Juncus* spp. were also present and are typically associated with riparian habitats and bogs (Cody,

486 2000). In contrast, the remains of *Papaver* spp. (poppies) and *Polygonum bistorta* (Figure 4 l),
487 which favor drier open slopes (Hulten, 1968), were also present in the bison skull cavity. The
488 largest number of plant macrofossils from the skull cavity was the mustard and *Draba*-type seeds
489 (Figures 4 m and 5), which are from a large and very diverse family making it difficult to use
490 these specimens to characterize paleoecological conditions (Cody, 2000; Hulten, 1968).
491 However, many of the species from this group are typical of open slopes, gravel and/or sandy
492 river banks (Cody, 2000). In addition, there is a portion of grasses (Poaceae) (Figure 4 k) (and
493 *Carex* Figure 4 i and j) that are typical of tundra or steppe ecosystems in the Arctic, and are
494 consistent with an open landscape with no large shrubs (Hulten, 1968). The burial occurred in a
495 time scale that prevented lots of skeletal disarticulation by scavengers but allowed some
496 activities by insects in an energy regime allowed deposition of sand but not coarser sediment.

497

498 **3.3.2 Fossil insect remains**

499

500 Analysis of the skull cavity of UAMES 29458 revealed the presence of insect remains, including
501 complete or incomplete blowfly puparia (Calliphoridae) (n = 15, UAMES 52319-52330). From
502 their excellent state of preservation, a determination at the species level was possible and the
503 taxon that colonized the bison at the time of its death was identified as the northern blowfly
504 *Protophormia terraenovae* (Robineau-Desvoidy) (Figure 4 a-e). With the exception of 4
505 fragmentary specimens, all the puparia were complete and unhatched indicating that the life
506 cycle was interrupted before adult emergence. An attempt to open two fossil puparia (#29458c,
507 #29458g), in order to find a possible nymph and to observe its maturity stage, proved
508 unsuccessful since the pupa had disintegrated inside.

509 Partial abdomen remains of a carabid beetle (Pterostichinae: cf. *Pterostichus* sp.) were
510 also found inside the skull (UAMES 52334; Figure 4 f). Thirty-five *Pterostichus* species occur in
511 Alaska (Bousquet et al., 2013). Some representatives of this genus (i.e. *Pterostichus costatus*
512 Ménériés), live in the damp peaty areas of lowland tundra regions (Lindroth, 1966). Other insect
513 remains belonging to several distinct orders were also recovered from inside the skull: a
514 complete wing of Psylloidea (Homoptera) (UAMES 52331; Figure 4 g); a cephalic capsule of a
515 larval Chironomidae (Diptera), an incomplete elytron of Elaphrinae (Coleoptera, Carabidae)
516 (UAMES 52332; Figure 4 h) and finally, some disarticulated coleopteran remains, too

517 fragmented to be identified. The presence of a psylloidean species in this context is not
518 surprising since fossil remains of the three main plants (*Salix*, *Betula*, *Polygonum*) exploited by
519 these insects were preserved evidenced within the skull cavity of the bison. The larval stages of
520 chironomids develop in almost any aquatic or semiaquatic habitat, both standing and flowing
521 waters, but also occur in tree-holes, rotting vegetation, and damp soils. Finally, the presence of
522 *Elaphrus* sp. (*cf. trossulus* Semenov) (UAMES 52333; Figure 4 h), another ground beetle, is
523 recorded. The species belonging to this genus are representative of riparian communities. Adults
524 of all species of *Elaphrus* live along rivers, small streams, swamps, sloughs, or bogs, which is
525 fully consistent with the bison discovery site. Overall, these taxa are typical of mesic to wet
526 tundra habitats at the time of burial.

527

528 **3.4 Isotopic analyses:**

529

530 The $\delta^{13}\text{C}$ and $\delta^{15}\text{N}$ values from the collagen sample were -20.0‰ (± 0.6) and 4.2‰ (± 0.1),
531 respectively. The $\delta^{13}\text{C}$ value is consistent with a diet of vegetation consists of plants using C_3
532 photosynthesis in a relatively open environment (Drucker et al., 2008). The $\delta^{15}\text{N}$ value is
533 consistent with values from other bison specimens dated to interstadial conditions, and contrast
534 with stadial conditions, which can have higher values (Hedges et al., 2004; Rabanus-Wallace et
535 al., 2017). Based on an 8-10 year collagen turn-over rate (Hedges et al., 2007), the collagen
536 would exclude the higher $\delta^{15}\text{N}$ values from this individual's early life based on analyses of the
537 horn sheath (described below), and thus the bone collagen and horn can be considered in the
538 same range. The mean horn keratin $\delta^{13}\text{C}$ value was slightly lower than the collagen values (mean
539 $\delta^{13}\text{C}$ value $-21.3\text{‰} \pm 1.1$; -20.0‰ respectively), which is consistent with the difference in
540 fractionation factors associated with the two different tissue types (keratin $\Delta = 3.1\text{‰} \pm 0.3$;
541 collagen $\Delta = 5.1\text{‰} \pm 0.3$ (Drucker et al., 2008)).

542 The mean $\delta^{15}\text{N}$ value from analyses of the horn keratin ($4.6\text{‰} \pm 1.1$) was similar to the
543 $\delta^{15}\text{N}$ value from the collagen value ($4.2\text{‰} \pm 0.1$). The periodicity of the isotopic fluctuations in
544 the horn sheath (Figure 6) appears to reflect annual cycles because the number of oscillations (n
545 $= 11$) is consistent with the number of observed annual growth layers observed from the horn
546 (11-12). The first two oscillations (~ 2 years) likely correspond with the period covered by the
547 tooth record (~ 2.5 years) from the same specimen (described below). These apparently annual

548 fluctuations would be consistent with the peaks in $\delta^{15}\text{N}$ values reflecting a seasonal shift to
549 greater nutritional stress and a more water-limited plant diet during the winter 2020). Shortly
550 before the death of the bison, the $\delta^{15}\text{N}$ values from the horn sheath increases (Figure 6), which
551 would correspond with a transition from summer to winter that is observed in modern bison from
552 Alaska (Funck et al., 2020), indicating the bison may have died in the late summer/early fall.
553 Two peaks in the $\delta^{15}\text{N}$ values from the horn sheath occurred towards the start of the life of the
554 bison and the second of these corresponds with a decrease in $\delta^{13}\text{C}$ values from the horn sheath.
555 These features are consistent with periods of nutritional stress (Funck et al., 2020). Most notably,
556 this pattern seems consistent with catabolism and the use of lipid reserves respectively (Funck et
557 al., 2020). A marked decrease in $\delta^{13}\text{C}$ values is evident in the year prior to the bison's death,
558 which also seems consistent with the use of the animal's lipid reserves (Funck et al., 2020).

559 The results of the $^{87}\text{Sr}/^{86}\text{Sr}$ ratio analyses ($n = 33$) from specimen UAMES 29458 (Table
560 2), with an analytical precision of 0.00001, show a mean $^{87}\text{Sr}/^{86}\text{Sr}$ ratio from the first molar (M1)
561 of 0.71139 (± 0.00028). These values are consistent with the rodent teeth values from the Arctic
562 Coastal Plain, which range from 0.70940 to 0.71107 (Table 3, Figure 7). The mean $^{87}\text{Sr}/^{86}\text{Sr}$ ratio
563 from the M2 was higher compared to the values from the M1 ($p < 0.000$, t.test), averaging at
564 0.71206 (± 0.00025). The mean $^{87}\text{Sr}/^{86}\text{Sr}$ value from the M3 was 0.71308 (± 0.00008) and was
565 higher than the values from both the M1 and M2 ($p < 0.000$, t.test). The range of the M3 values
566 was similar to the values found from the modern rodents found in the foothills of the Brooks
567 Range mountains (Table 3) (from 0.7137 to 0.7205) (Figure 8). Based on the bedrock $^{87}\text{Sr}/^{86}\text{Sr}$
568 model (Bataille and Bowen, 2012), the expected $^{87}\text{Sr}/^{86}\text{Sr}$ ratio at the place of death of specimen
569 UAMES 29458 was ~ 0.70982 (Figure 8). Overall, the M1, M2 and M3 sequential data show a
570 marked increase in $^{87}\text{Sr}/^{86}\text{Sr}$ ratios throughout the tooth sequence ($p < 0.000$, ANOVA) (Figure
571 7).

572 The mean $\delta^{18}\text{O}$ value across all teeth samples from specimen UAMES 29458 ($n = 30$)
573 was -21.1 ‰ (± 0.4) vs. VPDB (with an analytical precision of 0.2 ‰) (Table 4). Values were
574 highly variable across the M1-M3 sequence (Figure 7) ranging from -18.4 ‰ to -26.5 ‰ , but
575 were not significantly different between teeth ($p = 0.34$, ANOVA). The values appear to cycle
576 through approximately two full years, with three peaks representing summers, which seasonally
577 have higher $\delta^{18}\text{O}$ values (Velivetskaya et al., 2016) and separated by two cooler periods with
578 lower values (Figure 7).

579 The mean $\delta^{13}\text{C}$ value of the enamel calcium carbonate from the teeth of specimen
580 UAMES 29458 was -11.0‰ (± 2.0) (with an analytical precision of 0.03) and had a relatively
581 small range of values (-10.3‰ to -11.7‰) (Table 4), which are consistent with a C_3 diet.
582 Typical values for C_3 plants are $\sim -27\text{‰}$ (Wooller et al., 2007) and the difference between animal
583 diets and tooth calcium carbonate is $\Delta +14.6$ - (Cerling and Harris 1999; Passey et al. 2005).
584 Overall the $\delta^{13}\text{C}$ values started at their lowest during early life (M1) and gradually became higher
585 in the M2 ($-11.1\text{‰} \pm 0.2$) and M3 ($-10.5\text{‰} \pm 0.1$) ($p < 0.000$, ANOVA), a trend that appears to
586 correlate with the temporal shift from lower to higher $^{87}\text{Sr}/^{86}\text{Sr}$ ratios from the same teeth (Figure
587 7).

588

589 ***3.5 aDNA analyses:***

590

591 We generated 1.15 million reads from the unenriched library of UAMES 29458 (raw reads
592 available at the NCBI Short Read Archive under BioProject PRJNA61324), which had an
593 endogenous DNA content of 15.4% based on reads aligning to the cow genome. The relative
594 mapping frequency ratio between the X chromosome and autosomes was 0.528, with a range of
595 0.493-0.561 across all 29 autosomes (Table 5). This is consistent with UAMES 29458
596 representing a genomic male individual.

597 A full mitochondrial genome (JK319) was generated from the enriched library, with an
598 average coverage of $139\times$ (Genbank: MN549280). The phylogenetic placement of the UAMES
599 29458 mitochondrial genome was marginally impacted by the minimum age prior used, and was
600 found either to fall at the base of Clade 2 (prior of 50 kya BP) or to be sister to MS002 within
601 bison mitochondrial Clade 2 (all other tested priors) (Figure 9, Table 6). The inclusion or
602 exclusion of MS022 did not affect the phylogenetic placement of UAMES 29458. Across all
603 analyses, the age of UAMES 29458 was estimated to be ~ 33 -87 kya BP (Table 6). Analyses with
604 MS022 excluded generally yielded slightly older age estimates, but varying the minimum age
605 prior did not greatly impact this individual's maximum estimated age (range of ~ 81 -87 kya BP
606 across all analyses). This suggests that the priors did not drive the estimated age results.

607 Mapped reads from both the unenriched (primarily nuclear) and enriched (mitochondrial)
608 DNA libraries exhibit damage patterns characteristic of authentic aDNA, including short DNA
609 fragments and elevated relative deamination frequencies at the ends of reads (Figure S4).

610

611 **4. Discussion:**

612

613 ***4.1 Constraining a chronological age for UAMES 29458:***

614

615 Specimen UAMES 29458 provides several lines of evidence that can be used to constrain the
616 individual's chronological age (Figure 11). The radiocarbon dates from the keratin and the blow
617 fly puparium (chitin) are nearly identical ($46,000 \pm 1100$ ^{14}C yrs and $46,800 \pm 1200$ ^{14}C yrs –
618 inside and outside the range for calibration, respectively). Keratin is a structurally dense tissue
619 and less susceptible to contamination than collagen (Taylor et al., 1995). The blow flies *P.*
620 *terraenovae*, which colonizes a corpse within hours or days following death, seemed a good
621 candidate for precise ^{14}C dating of specimen UAMES 29458. The congruence of the keratin and
622 chitin ^{14}C dates lends support for a finite age of approximately $46,900$ ^{14}C yrs. In contrast, the
623 radiocarbon dates from collagen and from plant material are non-finite. Collagen, from porous
624 bone material, can be contaminated or degraded. The sample from the bone of UAMES 29458
625 was also run on a lower energy ^{14}C instrument, which cannot discriminate low levels of ^{14}C from
626 old samples compared with the chitin and keratin, which were run on a more powerful
627 instrument. The radiocarbon date of the plant material and its apparent older age compared to the
628 puparium and keratin is difficult to interpret. The plant material recovered from the skull was
629 specifically selected because it was a delicate herbaceous structure that would not have
630 experienced substantial reworking or be influenced by variations in carbon sources that can
631 occur in aquatic plants (Marcenko et al., 1989). However, the radiocarbon date of the plant was
632 determined to be non-finite ($>49,000$) and could have been reworked from older sediments.
633 Given that the dates from keratin and chitin are on the margins of radiocarbon limits we must
634 consider two possibilities; first, that the finite dates are accurate, or second, that these dates are
635 not distinguishable from non-finite dates.

636 Other evidence supports the hypothesis that UAMES 29458 dates are finite in age.
637 Environmental information from the $\delta^{18}\text{O}$ values from the bison specimen and plant macrofossils
638 add further dimensions that help constrain the chronological age estimation for UAMES 29458.
639 The mean $\delta^{18}\text{O}$ value (as VSMOW) from analyses of the bison's molars is -3.9 ‰ (± 1.2) lower
640 than the mean modern precipitation values. In contrast, full stadial $\delta^{18}\text{O}$ values for precipitation

641 tend to be around -8 ‰ lower than modern precipitation values (Bowen, 2018; Gaglioti et al.,
642 2017; Meyer et al., 2010; Rasmussen et al., 2014). The $\delta^{18}\text{O}$ values from UAMES 29458
643 therefore indicate that although the climate was slightly colder than modern it was not full stadial
644 (Figure 11). The finite radiocarbon date from the keratin coincides with a period of time that had
645 an offset in $\delta^{18}\text{O}$ values of $\Delta -3.9$ ‰ (± 1.2), between 44,380 cal yrs BP and 46,880 cal yrs BP
646 (Rasmussen et al., 2014). This inference that the bison specimen may have lived during a more
647 moderate (interstadial) climate is also supported by the plant macrofossils and insect remains
648 found in the skull, which represent a typical flood plain in tundra ecosystems of the Arctic.
649 However, as stated above, the plant remains may not be exactly contemporaneous with the
650 specimen.

651 The Bayesian molecular age estimate for the specimen was between ~33-87 kya BP,
652 which is consistent with the radiocarbon ages and corresponds to Marine Isotope Stage (MIS) 3
653 through to MIS 5b (Lisiecki and Raymo, 2005). Although the results of this analysis are not
654 informative as to whether UAMES 29458 is of older radiocarbon finite or non-finite age, they do
655 suggest that, if the individual were radiocarbon non-finite, it lived after MIS 5e. The finite
656 radiocarbon age from the bison's keratin is within the range of this molecular-clock derived age
657 estimate, which could narrow the age estimate to within MIS 3 (29-57 kya BP). Our
658 phylogenetic analyses show that UAMES 29458 belonged to bison mitochondrial clade 2
659 (Heintzman et al., 2016). This lineage did not contribute to extant bison diversity, and instead
660 became extinct during the late Holocene, by as long as ~400 years ago (Heintzman et al., 2016;
661 Shapiro et al., 2004). Given the varied methods used for dating this specimen, it is expected that
662 there might be some disagreement between results. However, the two nearly identical dates from
663 the chemically stable portions associated with the specimen (i.e. keratin and insect chitin, 46,000
664 ± 1100 ^{14}C yr BP and 46,800 ± 1200 ^{14}C yr BP, respectively) provide support for this as a finite-
665 aged specimen very close to the limit of radiocarbon dating. This age is congruent with an
666 appropriate climatic period suggested by the $\delta^{18}\text{O}$ values (Figure 11) and the macrofossil
667 assemblage of flora.

668

669 ***4.2 Life history of an individual steppe bison:***

670

671 Multiple lines of evidence suggest that specimen UAMES 29458 was a large bull that was 11 to
672 12 years old at the time of death. Present-day male bison of this age are typically lone bulls,
673 either in or just past their prime (Maher and Byers, 1987; Soper, 1941). During his life, this
674 individual incurred injury to a rib and the bone callous clearly indicates it healed (Figure 3c).
675 This type of injury typically occurs in present-day bison during the rut when bison compete for
676 access to females (Lott, 1971). In addition to this evidence of injury, the early stages of this
677 bison's life, recorded as the $\delta^{15}\text{N}$ values from the horn sheath (Figure 6), could indicate some
678 periods of nutritional stress. Increases in $\delta^{15}\text{N}$ values in the tissues of bison can represent
679 stressors, such as starvation, illness, or long-distance movement (Funck et al., 2020). Shifts in
680 $\delta^{15}\text{N}$ values are generally used to determine changes in the trophic level (Post, 2002), an
681 interpretation that is not appropriate for a herbivore, except during breast feeding when an
682 juvenile is essentially a trophic level above their mother (Gadbury et al., 2000; Reitsema and
683 Muir, 2015). However, during nutritional stress, such as a hard winter (Funck et al., 2020) or
684 nutritional transition like weaning (Fuller et al., 2003), an animal can break down its muscles to
685 build new proteins, during which tissues fractionate and lead to elevated $\delta^{15}\text{N}$ values (Lee et al.,
686 2012). The bison specimen analyzed here exhibited two periods of elevated $\delta^{15}\text{N}$ values towards
687 the start of its life (Figure 6). Horn stubs begin developing in utero but do not solidify into horn
688 spikes until the calves are older (Wiener et al., 2015). The two periods of higher $\delta^{15}\text{N}$ values
689 likely occurred in the first 2-3 years of life, overlapping with some of the time periods
690 represented by the molar development, which was used to produce the $\delta^{18}\text{O}$ values and $^{87}\text{Sr}/^{86}\text{Sr}$
691 ratios. This allows us several lines of evidence for interpreting what early life was like for this
692 bison.

693 The interpretation of intra-tooth serial samples as a measure of change over time requires
694 an understanding of how teeth develop and mineralize. For example, the molars of bison have
695 been shown to grow over 2 to 2.5 years (Gadbury et al., 2000; Higgins and MacFadden, 2004;
696 Velivetskaya et al., 2016) and the pattern of molar eruption occurs in a particular sequence and
697 time in an animal's life. As each molar develops, discrete layers of enamel are laid down and
698 retain the isotopic composition of conditions at each point in time. However, as a tooth develops
699 it continues to mineralize over 6 to 7 months leading to a degree of isotopic averaging (Balasse,
700 2002; Montgomery et al., 2010). As a result, changes that may appear progressive could in fact
701 occur over much shorter periods of time and the exact timing of tooth development and

702 mineralization can be subject to some degree of variation between individuals and species.
703 However, Velivetskaya et al. (2016) used high-resolution sampling for analysis of $\delta^{18}\text{O}$ values to
704 pinpoint the timing of tooth development in two late-Pleistocene steppe bison from the Middle
705 Urals, Russia and found it to be close to those of present-day bison. Seasonal oscillation in $\delta^{18}\text{O}$
706 values can also be compared to those of present-day animals to track the speed of tooth
707 development.

708 The M1 is formed in utero and shortly after birth (Bernard et al., 2009; Widga et al.,
709 2010), and thus represents the mother's home range and the calving grounds. The M1 formation
710 likely corresponds with the timing of the first $\delta^{15}\text{N}$ value peak (Figure 6). The $^{87}\text{Sr}/^{86}\text{Sr}$ ratios
711 from the M1 had less variation than the M2 suggesting the mother remained in a relatively
712 consistent geological area. When the M1 $^{87}\text{Sr}/^{86}\text{Sr}$ ratios are compared to bioavailable $^{87}\text{Sr}/^{86}\text{Sr}$
713 ratios from the region, it appears that this bison began life on the Alaska coastal plain (Figure 8).
714 Contemporary caribou from similar regions of Alaska currently use the coastal plain as calving
715 grounds, taking advantage of the emerging graminoids and open terrain (Fancy et al., 1990; Post
716 and Forchhammer, 2008). Subsequently, they move to higher ground to avoid insects and to take
717 advantage of abundant lichens that sustain them during non-calving seasons (Fancy et al., 1990).
718 Bison calves are dependent on milk for the first ~5 months and gradually stop suckling over 9-21
719 months (Green et al., 1993). So the first peak in $\delta^{15}\text{N}$ values from the horn (Figure 6) likely
720 corresponds to this M1 period and could be interpreted as a maternal/weaning signal (Gadbury et
721 al., 2000; Reitsema and Muir, 2015), either attributed to the bison being at a higher trophic level
722 than its mother from which it was nursing, or the effect of weaning and the nutritional stress that
723 it may have imparted (Fuller et al., 2003).

724 After the period of initial relative geographic stability inferred from the $^{87}\text{Sr}/^{86}\text{Sr}$ ratios in
725 the M1, which likely represented the first half-year of life, the bison seems to have dispersed into
726 a new geographic area during its second summer according to the $^{87}\text{Sr}/^{86}\text{Sr}$ ratios from the M2
727 and M3. The M2 development starts at ~2 to 3 months of age and continues for 12-15 months
728 (Gadbury et al., 2000; Velivetskaya et al., 2016). The M3 subsequently develops from the
729 beginning of the second summer after weaning, ~10-11 months until the age of about 2 to 2.5
730 years (Gadbury et al., 2000; Velivetskaya et al., 2016). Comparisons of the bison's $^{87}\text{Sr}/^{86}\text{Sr}$
731 ratios from the M2 and M3 to bioavailable $^{87}\text{Sr}/^{86}\text{Sr}$ ratios from the region indicate that the bison
732 may have moved into the foothills of the Brooks Range (Figure 1 and Figure 8). The second peak

733 in $\delta^{15}\text{N}$ values from the analyses of the horn sheath (Figure 6) could correspond to mobility on
734 the landscape, which seems to have occurred during this period. A study on present-day wood
735 bison in Alaska (Funck et al., 2020) found that bison that traveled long distances, or experienced
736 nutritional stress, produced elevated $\delta^{15}\text{N}$ values due to the energetic costs of travel. The horn
737 $\delta^{13}\text{C}$ record begins relatively low shortly before this point, which could be related to the bison
738 beginning to draw on the bodies lipids which have lower $\delta^{13}\text{C}$ values (DeNiro and Epstein, 1977;
739 Rode et al., 2018). This offset follows the same pattern found in a modern wood bison
740 experiencing a dispersal related dietary stress (Funck et al., 2020). In the present study, the tooth
741 carbonate $\delta^{13}\text{C}$ values show an overall increase (+1 ‰) during this same period (~2.5 years),
742 consistent with a change from a wetter environment to a drier one (Wooller et al., 2007), which
743 also seems to correspond with a shift towards the higher and drier elevations of the foothills
744 compared to the wetter, lower reaches, of the coastal plain. Later in the bison's life, after the
745 record preserved in the molars is fully mineralized (~2.5 years), we lose track of the specimen's
746 geolocation based on the $^{87}\text{Sr}/^{86}\text{Sr}$ record. However, this bison must have eventually returned to
747 the coastal plain to the location where he eventually died and was found (Figure 1).

748 In contrast to the tooth record, the horn sheath continues to develop over approximately
749 the lifetime of the individual. The $\delta^{15}\text{N}$ fluctuates through what appear to be seasonal oscillations
750 of slightly more elevated $\delta^{15}\text{N}$ values in the winter, likely due to nutritional stress during this
751 season, then lower $\delta^{15}\text{N}$ values during more favorable summers, interpreted based on isotopic
752 patterns exhibited in present-day bison from Alaska (Funck et al., 2020). Present-day wood bison
753 south of the Brooks Range in Alaska only had changes in $\delta^{15}\text{N}$ values during particularly hard
754 winters (Funck et al., 2020). Thus, these winters were likely harder than the conditions
755 experienced by present-day analogous populations. Applying this seasonal pattern implies that
756 the sample closest to the horn core (i.e. the period leading to the animal's death) represented the
757 start of the transition from the summer to winter. This indicates that the bison was not
758 experiencing unusual nutritional stress and did not appear to have been in a weakened state prior
759 to death. Other potential causes for changes in $\delta^{15}\text{N}$ values in herbivores could include changes
760 in the seasonal $\delta^{15}\text{N}$ values of forage and seasonal movement to regions with very different
761 baseline $\delta^{15}\text{N}$ values. Our data indicates that this bison individual did move substantially across
762 the landscape. However, the tooth record of paleomobility is not long enough to cover the longer
763 record represented by the horn sheath data. We find that our interpretation of the $\delta^{15}\text{N}$ values as

764 a marker in terms of changes in the degree of nutritional stress is in some ways supported by the
765 $\delta^{13}\text{C}$ data from the horn sheath. For example, the low $\delta^{13}\text{C}$ values from the horn sheath in the last
766 year of life, relative to the rest of the record from the horn, could indicate that the animal may
767 have begun to draw on its lipid reserves (Funck et al., 2020). Although in some animals these
768 isotopic shifts occurs only at extreme thresholds of starvation this is a more common strategy in
769 animals that have large fat and muscle reserves for winter use, such as bison (Funck et al., 2020).

770 The degree of mobility of the bison specimen analyzed, based on the $^{87}\text{Sr}/^{86}\text{Sr}$ ratio data
771 from the North Slope specimen, is relatively high compared to data from other ancient and
772 present-day bison (Figure 10, Table 7; Britton et al., 2011; Glassburn, et al., 2015; Julien et al.
773 2012; Widga et al., 2010). Although the range of $^{87}\text{Sr}/^{86}\text{Sr}$ ratios cannot be directly compared,
774 because variability is highly dependent on the geological heterogeneity of a landscape that
775 individuals inhabit it is worth considering this bison in the context of others analyzed using the
776 similar methods. Britton et al. (2011) examined a single bison from western France dating to
777 $49,000 \pm 5000$ BP and demonstrated high fidelity to an area, with almost no variability in
778 $^{87}\text{Sr}/^{86}\text{Sr}$ ratios despite a variable geological environment. Julien et al. (2012) found that steppe
779 bison from the Last Glacial Maximum (LGM) (~ 20.5 kya BP) in Amrosievika in Eastern
780 Ukraine had a $^{87}\text{Sr}/^{86}\text{Sr}$ range of 0.00074 (Julien et al., 2012). This range was attributed to the
781 low degree of variability to minimal mobility on the landscape because there was no signals from
782 mixed geology as close as 20 km to the south-west of the site where the bison were found (Julien
783 et al., 2012). A study of bison herds on the Great Plains of North America from the Middle
784 Holocene indicated that bison also had limited seasonal mobility (<50 km), while inter-annual
785 movement of herds over ~ 4 -5 yrs moved further afield (<500 km) (Widga et al., 2010a). In
786 contrast, present-day *Bison bison* from the interior of Alaska, with an observed seasonal and
787 regional migration route of about a 100km, had a $^{87}\text{Sr}/^{86}\text{Sr}$ ratio range from 0.71714 to 0.71540
788 (0.00174) (Glassburn et al., 2018). Although these regions and studies cannot be quantitatively
789 compared because of difference in local geology (Bataille et al., 2020) we can still draw some
790 qualitative comparisons. The variability in $^{87}\text{Sr}/^{86}\text{Sr}$ ratio ranges among bison from different
791 localities and periods suggests that bison utilize different mobility strategies that are dependent
792 on (paleo)ecological conditions. The range of $^{87}\text{Sr}/^{86}\text{Sr}$ ratio variation from the North Slope bison
793 specimen analyzed here (0.00237) is relatively large compared to all these previous measures,
794 indicating that he was likely a gregarious individual who traveled some distance during his early

795 years of life. There is a large geological range in this region (Bataille et al., 2020) that this bison
796 appears to be utilizing. Future research could integrate genetic testing of sex from specimens to
797 determine if males and females used different mobility strategies.

798

799 ***4.3 Necrology and Biostratinomy:***

800

801 Evidence from the specimen UAMES 29458 helps shape a paleoecological picture leading up to
802 the individual's death, decomposition, and the mechanism of burial. The bones from the bison
803 specimen were overall in a state of excellent preservation as evidenced by the presence of intact
804 horn, hooves, fur, spinal cord, cartilage, and possible brain tissues. Specimens of this level of
805 completeness are extremely rare in Quaternary deposits. There were no obvious signs of the
806 cause of death, such as bite marks around the nose or neck, and all carnivore marks were related
807 to scavenging (Andersson et al., 2011) but predation cannot be ruled out. After death, the
808 specimen came to finally rest on his right side, which protected that side from scavenging, this is
809 further supported by the presence of vivianite. Vivianite deposits tended to be on the bone
810 surfaces that were exposed to the ground surface and root etching also tended to be present on
811 the surfaces of the bones that rested on the ground (Supplemental data).

812 Carnivore tooth marks are present at various locations on the specimen, indicating
813 scavenging of the bison carcass occurred post mortem (Figure 3 a and b and Supplemental data).
814 There are four major carnivore taxa present contemporaneously that could cause the type of
815 damage seen on UAMES 29458: *Arctodus simus* (short-faced bear), *Canis Lupus* (wolf),
816 *Homotherium serum* (scimitar cat), and *Panthera atrox* (American lion) (Fox-dobbs et al., 2008;
817 Schubert, 2010). The dentition marks (Figure 3) were consistently narrow punctures, which are
818 not consistent with the wide teeth of *A. simus* (Sorkin, 2006) or *H. serum* (Ewald et al., 2018).
819 The incisor punctures indicated that the space between the canines is at least 6 cm apart (Figure
820 3a, which is consistent with *P. atrox* (Baryshnikov and Boeskorov, 2001; Christiansen and
821 Harris, 2010). This may be out of the range of the smaller *C. lupus* (Sorkin, 2006), leaving large
822 *felidae* as the most likely scavenger. Further analysis of dentition morphometrics in predator
823 species would be useful for this type of taphonomic analysis. Indication of lion scavenging have
824 also been found on other preserved bison specimens from in Alaska (Guthrie, 1989). It is likely
825 that only one individual scavenger caused all of the damage based on the consistency in size of

826 the tooth marks of the 14 tooth marks with punctures. The 11 instances of gnawing are less
827 diagnostic but also appear consistent. The limited scavenging also supports a single scavenger, as
828 more individuals would require less time to remove meat, disarticulate the corpse, and scavenge
829 from a greater area of the carcass (Blumenschine, 1986). The carnivore appears to have
830 consumed the bison carcass and ate portions of the backstrap (meat along the top of the spine)
831 based on observed damage along the spinous processes of several vertebrae (Figure 3 a and b).
832 The carnivore also seems to have consumed the carcass from the inside of the body and likely ate
833 the internal organs and tenderloin based on damage to the costal cartilage, the distal ribs, the
834 transverse processes of the lumbar vertebrae, and the sacrum. In addition, the carnivore gnawed
835 the left humerus and likely removed the left scapula, in an attempt to get at the flesh of the left
836 fore-limb. Scavenging only seems to have occurred in high-value areas, supporting an inference
837 that the carcass was likely buried rapidly. In most contexts a carcass on an open landscape with
838 carnivores can be consumed and disarticulated within hours to a few days (Blumenschine, 1986).
839 It is for this reason that complete specimens are extremely rare. Thus, for this specimen to
840 preserve, something exceptional must have occurred to protect it. During the erosion that re-
841 exposed the bison it seems the left extremities of the front and hind limbs (phalanges, carpals,
842 tarsals, etc.) may have been lost due to erosional processes (Figure 2). These skeletal elements
843 would be the first to be exposed and vulnerable to gravity, weathering, and would have been
844 preferentially removed via taphonomic agents (e.g., eroded into the river and lost). These skeletal
845 elements of the lower extremities are also not associated with high food value flesh and likely
846 would not have been a target for scavenging.

847 The presence of the blow fly puparia recovered from inside the skull made it possible to
848 propose some "paleoforensic" hypotheses associated with postmortem events. Blow flies figure
849 among the most relevant witnesses in forensic entomology in order to determine the time elapsed
850 since death, namely the postmortem interval (PMI) because blow flies (Calliphoridae) are the
851 first and predominant organisms to colonize a body after death. Within hours of death, these
852 insects are attracted to the smell of the decomposing remains, which are both a site for laying
853 eggs and a source of protein for larval development. Under normal circumstances, egg laying
854 occurs soon after death (1–3 days) (Gomes et al., 2006). The favored egg-laying sites are the
855 natural openings of the body (mouth, eyes, anus) as well as any wounds present on the corpse
856 (Gomes et al., 2006). The species preserved on the carcass *Protophormia terraenovae* (Robineau

857 Desvoidy) is a Holarctic, cold-adapted species, present throughout northern Europe and Asia.
858 Very common in the cooler high latitude regions and notably in the Arctic, representatives of this
859 species are found within 890 km of the North Pole (Smith, 1986). Experiments conducted by
860 Marchenko (2001) found that the development period of *P. terraenovae* (from egg to adult) is
861 relatively long. According to Warren and Anderson (2013), egg-carrying females of *P.*
862 *terraenovae* do not lay eggs at temperatures lower than 10.3°C. In the North Slope region,
863 temperatures only reach above 10°C during the summer period (<https://www.weatherbase.com>).
864 Insects, like all arthropods, are coldblooded and the duration of their life-cycle is primarily
865 temperature driven. Rate of development is species-specific and influenced by biotic (e.g.
866 maggot mass that can significantly accelerate rate of development) and environmental factors
867 (exposure of the carcass to sunlight or shade, rain, and wind). Following the biological data
868 provided by Marchenko (2001), and focusing on temperatures ranging from 11 to 18°C
869 (respectively the average minimal temperature required for laying eggs and the current maximum
870 temperatures recorded on the paleontological site), *P. terraenovae* development extends from 15
871 to 50 days (egg to pupal stage) and adult emergence from 24 to 78 days. In the case of UAMES
872 29458, all of the puparia were intact with no evidence of adult emergence.

873 The fact that the bison's skeleton was almost complete and articulated, and not fully
874 scavenged by carnivores suggests that the fly pupal stage intervened fairly quickly, indicating
875 relatively high temperatures at the time of death (e.g., at 18°C, the pupal stage would have
876 started on the 15th day). The bison carcass was then quickly covered with sediment or snow
877 precluding further access to predators; however, a few centimeters of soil cover would not
878 prevent the development and emergence of flies (Balme et al., 2012). Trapped in the skull, the
879 pupae would have preserved in situ. The presence of unhatched fly puparia of *P. terraenovae*
880 recovered from the bison individual would suggest that its carcass had been subaerially exposed
881 for at least 2 weeks before the life cycle was interrupted either due to a more complete burial or
882 freezing. The fact that the carcass was little affected by scavengers over this period might be
883 explain by low scavenger density on site, high carcass availability or because the bison's remains
884 were only accessible to flying insects and not by terrestrial scavengers (e.g. carcass partially
885 exposed in river water). Finally, we can argue that the ambient temperature was very likely over
886 10°C when the fly infestation occurred, requiring the events to occur during a warm period of the

887 year. This warm period seems to have been at the transition from summer to winter, based on the
888 isotopic evidence from the horn sheath.

889 Fluvial sediments including plant macrofossils likely entered the skull after this initial
890 burial during which the *P. terraenovae* puparia developed. The plant macrofossils recovered
891 from inside the skull and neural canal are unlikely penecontemporaneous with the death of this
892 bison individual, but could indicate an overall glimpse of the surroundings. The macrofossil
893 assemblage of plants is consistent with an Arctic flood plain. The immediate surrounding of the
894 river was probably covered in moss, low shrubs, and bogs (Figure 5). Further away from the
895 banks of the river were likely drier tundra with grasses, sedges, and a variety of tundra flowers
896 including *Papaver* sp., *Polygonum bistorta*, and *Draba* type (Figure 5). Overall, the plant
897 assemblage is more typical of a mesic tundra than a steppe and possibly originated from an inter-
898 glacial or interstadial environment (Gaglioti et al., 2018).

899 Overall, we conclude that this bison died on a flood plain during the warm period prior to
900 the onset of winter and fell on to its right side. A carnivore, possibly a large *felidae*, quickly
901 consumed high-value areas of meat and blow flies swiftly laid eggs within the skull. Alluvial
902 sediments or possibly snow then quickly buried the carcass before the carcass could be further
903 disarticulated. At least two weeks passed before temperatures inside the carcass or the oxygen
904 availability fell too low for the puparia to continue developing.

905

906 **5. Conclusion:**

907

908 Our multi-proxy paleoecological evidence from UAMES 29458 fills out the details of an
909 individual bison's life and death in the Arctic, where bison were once a dominant herbivore.
910 Combining serial isotope analyses with aDNA allowed us to combine mobility information with
911 genealogical information, and to place the individual within bison meta-population dynamics
912 over millennia. This augments a paleoecological picture based on the physical evidence of the
913 skeletal remains alone, providing a more vivid image of a highly mobile individual moving
914 across the North Slope of Alaska. The mitochondrial lineage of this bison is one that thrived in
915 Beringia but ultimately died out. Our multiproxy evaluation indicates that this bison likely lived
916 during an interstadial period, which in some ways may have been somewhat similar to today.
917 Strontium isotope data from the specimen indicates that he dispersed across the Northern Alaska

918 landscape from possible calving grounds located on the Arctic coastal plain to the foothills of the
919 Brooks Range in early life and ultimately back to his place of death on the Arctic coastal plain.
920 Nitrogen isotopes from the horn sheath indicate that the mobility of his early life may have
921 resulted in significant nutritional stress, and that this individual suffered somewhat harsher
922 winters than those on the North Slope today. The taphonomic analysis revealed that this bison
923 was scavenged in parts of high nutritional value, which was followed by a rapid burial in a
924 riverine environment.. In this case, a multiproxy approach has uncovered a life history and
925 detailed examination of a member of a dominant Pleistocene species in the Arctic.

926

927 **Acknowledgments:**

928

929 First and foremost, we recognize and are very grateful for the efforts of Dr. Dannial Mann and
930 Dr. Pamela Groves in discovering, excavating, and transporting this exceptional specimen,
931 affectionately known as ‘Bison Bob’ to the UAMN. Without them none of this work would have
932 been possible and we thank them for discussions. The bison specimen was collected during
933 fieldwork directed by Mike Kunz and funded by the Bureau of Land Management. Kathrine
934 Anderson at the Museum of the North Earth Sciences managed curating the bison specimen. In
935 addition, she assisted Stormy Fields and Juliette Funck in preparing the specimen for taphonomic
936 analysis. Aren Gunderson helped locate and select rodent specimens at the Museum of the North
937 Mammalogy. Dr. Diego Fernandez at the University of Utah conducted strontium isotope
938 analysis. We thank Tim Howe at the Alaska Stable Isotope Facility for assistance conducting the
939 stable isotope analyses of the specimen. Amanda Barker provided support and advice on
940 chemistry preparation. Radiocarbon analysis was conducted by W. M. Keck Carbon Cycle
941 Accelerator Mass Spectrometry Laboratory by Dr. John Southon, who provided expertise in
942 evaluating radiocarbon results from the bison specimen. The Bureau of Land Management
943 oversaw specimen management and permitted destructive analysis of necessary materials for this
944 study. The 2016 and 2017 David and Rachel Hopkins Fellowship provided funds for strontium
945 analysis. Dr. Beth Shapiro was supported by IMLS MG-30-17-0045-17. Gemma Murray and Dr.
946 Peter Heintzman were partially supported by NSF DEB 1754451. Joshua D. Kapp assisted in the
947 aDNA analysis. Dr. Derek Sikes, Dr. Denise Gemmellaro, and Dr. Martin Hall were all

948 contacted for their expertise with forensic entomology. We thank two anonymous reviewers for
949 their constructive input that improved this research.

950

951 **References:**

952 Andersson, K., Norman, D., Werdelin, L., 2011. Sabretoothed carnivores and the killing of large
953 prey. PLoS One 6, 8–13. <https://doi.org/10.1371/journal.pone.0024971>

954 Balasse, M., 2002. Reconstructing dietary and environmental history from enamel isotopic
955 analysis: Time resolution of intra-tooth sequential sampling. Int. J. Osteoarchaeol. 12, 155–
956 165. <https://doi.org/10.1002/oa.601>

957 Balasse, M., Bocherens, H., Mariotti, A., Ambrose, S.H., 2001. Detection of Dietary Changes by
958 Intra-tooth Carbon and Nitrogen Isotopic Analysis: An Experimental Study of Dentine
959 Collagen of Cattle (*Bos taurus*). J. Archaeol. Sci. 28, 235–245.
960 <https://doi.org/10.1006/jasc.1999.0535>

961 Balme, G.R., Denning, S.S., Cammack, J.A., Watson, D.W., 2012. Blow flies (Diptera:
962 Calliphoridae) survive burial: Evidence of ascending vertical dispersal. Forensic Sci. Int.
963 216, e1–e4. <https://doi.org/10.1016/j.forsciint.2011.07.017>

964 Bamforth, D.B., 1987. Historical Documents and Bison Ecology on the Great Plains. Plains
965 Anthropologist 32, 1–16. <https://doi.org/10.1080/2052546.1987.11909364>

966 Barbosa, I.C.R., Kley, M., Schaufele, R., Auerswald, K., Schroder, W., Filli, F., Hertwig, S.,
967 Schnyder, H., 2009. Analysing the isotopic life history of the alpine ungulates *Capra ibex*
968 and *Rupicapra rupicapra rupicapra* through their horns. Rapid Commun. Mass Spectrom.
969 23, 2347–2356. <https://doi.org/10.1002/rcm>

970 Baryshnikov, G., Boeskorov, G., 2001. The pleistocene cave lion, *Panthera spelaea* (Carnivora,
971 Felidae) from Yakutia, Russia. Cranium 18.

972 Bataille, C.P., Bowen, G.J., 2012. Sr / 86 Sr variations in bedrock and water for large scale
973 provenance studies. Chem. Geol. 304–305, 39–52.
974 <https://doi.org/10.1016/j.chemgeo.2012.01.028>

975 Bataille, C.P., Brennan, S.R., Hartmann, J., Moosdorf, N., Wooller, M.J., Bowen, G.J., 2014. A
976 geostatistical framework for predicting variability in strontium concentrations and isotope
977 ratios in Alaskan rivers. Chem. Geol. 389, 1–15.
978 <https://doi.org/10.1016/j.chemgeo.2014.08.030>

979 Bataille, C.P., Crowley, B.E., Wooller, M.J., Bowen, G.J., 2020. Advances in global bioavailable
980 strontium isoscapes. Palaeogeogr. Palaeoclimatol. Palaeoecol. 555, 109849.
981 <https://doi.org/10.1016/j.palaeo.2020.109849>

982 Berger, J., 2004. The last mile: How to sustain long-distance migration in mammals. Conserv.
983 Biol. 18, 320–331. <https://doi.org/10.1111/j.1523-1739.2004.00548.x>

- 984 Bernard, A., Daux, V., Lécuyer, C., Brugal, J.P., Genty, D., Wainer, K., Gardien, V., Fourel, F.,
985 Jaubert, J., 2009. Pleistocene seasonal temperature variations recorded in the $\delta^{18}\text{O}$ of *Bison*
986 *priscus* teeth. *Earth Planet. Sci. Lett.* 283, 133–143.
987 <https://doi.org/10.1016/j.epsl.2009.04.005>
- 988 Bigelow, N.H., Zazula, G.D., Atkinson, D.E., 2013. Plant Macrofossil Records: Arctic North
989 America, in: Elias, S.A., Mock, C.J. (Eds.), *Encyclopedia of Quaternary Science*. Elsevier,
990 Amsterdam, pp. 746–759.
- 991 Binford, L.R., 1981. *Bones: Ancient Men, Modern Myths*. Academic Press, New York.
- 992 Blumenschine, R.J., 1986. Carcass consumption sequences and the archaeological distinction of
993 scavenging and hunting. *J. Hum. Evol.* 15, 639–659. [https://doi.org/10.1016/S0047-](https://doi.org/10.1016/S0047-2484(86)80002-1)
994 [2484\(86\)80002-1](https://doi.org/10.1016/S0047-2484(86)80002-1)
- 995 Bocherens, H. (2003). Isotopic biogeochemistry and the paleoecology of the mammoth steppe
996 fauna.. In: Reumer, J. (Ed.), *Advances in Mammoth Research, Proceedings of the 2nd*
997 *International Mammoth Conference, Rotterdam*. DEINSEA. 9, 57–76.
- 998 Boeskorov, G.G., Potapova, O.R., Protopopov, A. V., Plotnikov, V. V., Agenbroad, L.D.,
999 Kirikov, K.S., Pavlov, I.S., Shchelchkova, M. V., Belolyubskii, I.N., Tomshin, M.D.,
1000 Kowalczyk, R., Davydov, S.P., Kolesov, S.D., Tikhonov, A.N., van der Plicht, J., 2016. The
1001 Yukagir Bison: The exterior morphology of a complete frozen mummy of the extinct steppe
1002 bison, *Bison priscus* from the early Holocene of northern Yakutia, Russia. *Quat. Int.* 406,
1003 94–110. <https://doi.org/10.1016/j.quaint.2015.11.084>
- 1004 Bousquet, Y., Bouchard, P., Davies, A.E., Sikes, D.S., 2013. Checklist of beetles (Coleoptera) of
1005 Canada and Alaska . Second edition. *Zookeys* 44, 1–44.
1006 <https://doi.org/10.3897/zookeys.360.4742>
- 1007 Bowen, G.J., 2018. *WaterIsotopes.org* [WWW Document]. Univ. Utah. Accessed: Dec. 2019.
- 1008 Brennan, S.R., Fernandez, D.P., Mackey, G., Cerling, T.E., Bataille, C.P., Bowen, G.J., Wooller,
1009 M.J., 2014. Strontium isotope variation and carbonate versus silicate weathering in rivers
1010 from across Alaska: Implications for provenance studies. *Chem. Geol.* 389, 167–181.
1011 <https://doi.org/10.1016/j.chemgeo.2014.08.018>
- 1012 Briggs, A.W., Good, J.M., Green, R.E., Krause, J., Maricic, T., Stenzel, U., Lalueza-fox, C.,
1013 Rudan, P., Brajković, D., Kućan, Ž., Rasilla, M. De, Fortea, J., Rosas, A., Pääbo, S., 2009.
1014 Five Neandertal mtDNA Genomes. *Science* (80-.). 325, 318–321.
- 1015 Britton, K., 2009. Reconstructing faunal migrations using intra- tooth sampling and strontium
1016 and oxygen isotope analyses : A case study of modern caribou (*Rangifer tarandus granti*).
1017 <https://doi.org/10.1016/j.jas.2009.01.003>
- 1018 Britton, K., Gaudzinski-Windheuser, S., Roebroeks, W., Kindler, L., Richards, M.P., 2012.
1019 Stable isotope analysis of well-preserved 120,000-year-old herbivore bone collagen from
1020 the Middle Palaeolithic site of Neumark-Nord 2, Germany reveals niche separation between
1021 bovids and equids. *Palaeogeogr. Palaeoclimatol. Palaeoecol.* 333–334, 168–177.

- 1022 <https://doi.org/10.1016/j.palaeo.2012.03.028>
- 1023 Britton, K., Grimes, V., Dau, J., Richards, M.P., 2009. Reconstructing faunal migrations using
1024 intra-tooth sampling and strontium and oxygen isotope analyses: a case study of modern
1025 caribou (*Rangifer tarandus granti*). *J. Archaeol. Sci.* 36, 1163–1172.
1026 <https://doi.org/10.1016/j.jas.2009.01.003>
- 1027 Britton, K., Grimes, V., Niven, L., Steele, T.E., McPherron, S., Soressi, M., Kelly, T.E., Jaubert,
1028 J., Hublin, J.J., Richards, M.P., 2011. Strontium isotope evidence for migration in late
1029 Pleistocene *Rangifer*: Implications for Neanderthal hunting strategies at the Middle
1030 Palaeolithic site of Jonzac, France. *J. Hum. Evol.* 61, 176–185.
1031 <https://doi.org/10.1016/j.jhevol.2011.03.004>
- 1032 Capo, R.C., Stewart, B.W., Chadwick, O.A., 1998. Strontium isotopes as tracers of ecosystem
1033 processes: theory and methods. *Geoderma* 82, 197-225 (pp.21).
1034 [https://doi.org/10.1016/S0016-7061\(97\)00102-X](https://doi.org/10.1016/S0016-7061(97)00102-X)
- 1035 Carlson, K., Bement, L.C., Carter, B.J., Culleton, B.J., Kennett, D.J., 2016. A Younger Dryas
1036 signature in bison bone stable isotopes from the southern Plains of North America. *J.*
1037 *Archaeol. Sci. Reports* 1–7. <https://doi.org/10.1016/j.jasrep.2017.03.001>
- 1038 Carter, L.D., 1981. A pleistocene sand sea on the alaskan arctic coastal plain. *Science* 211, 381–
1039 3. <https://doi.org/10.1126/science.211.4480.381>
- 1040 Cerling, T.E., Harris, J.M., 1999. Carbon isotope fractionation between diet and bioapatite in
1041 ungulate mammals and implications for ecological and paleoecological studies. *Oecologia*
1042 120, 347–363. <https://doi.org/10.1007/s004420050868>
- 1043 Christiansen, P., Harris, J.M., 2010. Craniomandibular morphology and phylogenetic affinities of
1044 *Panthera atrox*: implications for the evolution and paleobiology of the lion lineage. *J.*
1045 *Vertebr. Paleontology* 4634. <https://doi.org/10.1671/039.029.0314>
- 1046 Clark, P.U., Dyke, A.S., Shakun, J.D., Carlson, A.E., Clark, J., Wohlfarth, B., Mitrovica, J.X.,
1047 Hostetler, S.W., McCabe, A.M., 2009. The Last Glacial Maximum. *Science* (80-.). 325,
1048 710–714. <https://doi.org/10.1126/science.1172873>
- 1049 Cody, W.J., 2000. *Flora of the Yukon Territory, Second Edi.* ed. NRC Research Press, Ottawa,
1050 Ontario, Canada.
- 1051 Dabney, J., Knapp, M., Glocke, I., Gansauge, M.-T., Weihmann, A., Nickel, B., Valdiosera, C.,
1052 Garcia, N., Paabo, S., Arsuaga, J.-L., Meyer, M., 2013. Complete mitochondrial genome
1053 sequence of a Middle Pleistocene cave bear reconstructed from ultrashort DNA fragments.
1054 *Proc. Natl. Acad. Sci.* 110, 15758–15763. <https://doi.org/10.1073/pnas.1314445110>
- 1055 Delgiudice, G.D., Kerr, K.D., Mech, L.D., Seal, U.S., 2000. Prolonged winter undernutrition and
1056 the interpretation of urinary allantoin : creatinine ratios in white-tailed deer. *Can. J. Zool.*
1057 78, 2147–2155.
- 1058 DeNiro, M.J., Epstein, S., 1977. Mechanism of Carbon Isotope Fractionation Associated with
1059 Lipid Synthesis. *Am. Assoc. Adv. Sci.* 197, 261–263.

- 1060 Domínguez-Rodrigo, M., 1999. Flesh availability and bone modifications in carcasses consumed
1061 by lions: Palaeoecological relevance in hominid foraging patterns. *Palaeogeogr.*
1062 *Palaeoclimatol. Palaeoecol.* 149, 373–388. [https://doi.org/10.1016/S0031-0182\(98\)00213-2](https://doi.org/10.1016/S0031-0182(98)00213-2)
- 1063 Drucker, D., Bocherens, H., Bridault, A., Billiou, D., 2003. Carbon and nitrogen isotopic
1064 composition of red deer (*Cervus elaphus*) collagen as a tool for tracking
1065 palaeoenvironmental change during the Late-Glacial and Early Holocene in the northern
1066 Jura (France). *Palaeogeogr. Palaeoclimatol. Palaeoecol.* 195, 375–388.
1067 [https://doi.org/10.1016/S0031-0182\(03\)00366-3](https://doi.org/10.1016/S0031-0182(03)00366-3)
- 1068 Drucker, D.G., Bridault, A., Hobson, K. a., Szuma, E., Bocherens, H., 2008. Can carbon-13 in
1069 large herbivores reflect the canopy effect in temperate and boreal ecosystems? Evidence
1070 from modern and ancient ungulates. *Palaeogeogr. Palaeoclimatol. Palaeoecol.* 266, 69–82.
1071 <https://doi.org/10.1016/j.palaeo.2008.03.020>
- 1072 Drucker, D.G., Hobson, K. a, Ouellet, J.-P., Courtois, R., 2010. Influence of forage preferences
1073 and habitat use on ¹³C and ¹⁵N abundance in wild caribou (*Rangifer tarandus* caribou) and
1074 moose (*Alces alces*) from Canada. *Isotopes Environ. Health Stud.* 46, 107–21.
1075 <https://doi.org/10.1080/10256010903388410>
- 1076 Drummond, A.J., Suchard, M.A., Xie, D., Rambaut, A., 2012. Bayesian phylogenetics with
1077 BEAUti and the BEAST 1.7. *Mol. Biol. Evol.* 29, 1969–1973.
1078 <https://doi.org/10.1093/molbev/mss075>
- 1079 Elias, S.A., Berman, D., Alfimov, A., 2000. Late pleistocene beetle faunas of beringia: Where
1080 east met west. *J. Biogeogr.* 27, 1349–1363. <https://doi.org/10.1046/j.1365-2699.2000.00503.x>
- 1082 Elias, S.A., Crocker, B., 2008. The Bering Land Bridge: a moisture barrier to the dispersal of
1083 steppe-tundra biota? *Quat. Sci. Rev.* 27, 2473–2483.
1084 <https://doi.org/10.1016/j.quascirev.2008.09.011>
- 1085 Ewald, T., Hills, L. V., Tolman, S., Kooyman, B., 2018. Scimitar cat (*Homotherium serum*
1086 Cope) from southwestern Alberta, Canada. *Can. J. Earth Sci.* 55, 8–17.
1087 <https://doi.org/10.1139/cjes-2017-0130>
- 1088 Fancy, S.G., Pank, L.F., Whitten, K.R., Regelin, W.L., 1990. Seasonal movements of caribou in
1089 arctic Alaska as determined by satellite. *Rangifer* 10, 167.
1090 <https://doi.org/10.7557/2.10.3.850>
- 1091 Firth, C., Kitchen, A., Shapiro, B., Suchard, M.A., Holmes, E.C., Rambaut, A., 2010. Using
1092 time-structured data to estimate evolutionary rates of double-stranded DNA viruses. *Mol.*
1093 *Biol. Evol.* 27, 2038–2051. <https://doi.org/10.1093/molbev/msq088>
- 1094 Fisher, J.W., 1995. J.W. Bone surface modifications in zooarchaeology. *J. Archaeol. Method*
1095 *Theory* 2, 7–68.
- 1096 Flores, D., 1991. Bison Ecology and Bison Diplomacy: The Southern Plains from 1800 to 1850.
1097 *J. Am. Hist.* 78, 465. <https://doi.org/10.2307/2079530>

- 1098 Fox-dobbs, K., Leonard, J.A., Koch, P.L., 2008. Pleistocene megafauna from eastern Beringia :
 1099 Paleocological and paleoenvironmental interpretations of stable carbon and nitrogen
 1100 isotope and radiocarbon records. *Palaeogeogr. Palaeoclimatol. Palaeoecol.* 261, 30–46.
 1101 <https://doi.org/10.1016/j.palaeo.2007.12.011>
- 1102 Froese, D., Stiller, M., Heintzman, P.D., Reyes, A. V., Zazula, G.D., Soares, A.E.R., Meyer, M.,
 1103 Hall, E., Jensen, B.J.L., Arnold, L.J., MacPhee, R.D.E., Shapiro, B., 2017. Fossil and
 1104 genomic evidence constrains the timing of bison arrival in North America. *Proc. Natl. Acad.*
 1105 *Sci.* 114, 3457–3462. <https://doi.org/10.1073/pnas.1620754114>
- 1106 Fuller, B.T., Fuller, J.L., Sage, N.E., Harris, D.A., O’Connell, T.C., Hedges, R.E.M., 2005.
 1107 Nitrogen balance and $\delta^{15}\text{N}$: why you’re not what you eat during nutritional stress. *Rapid*
 1108 *Commun. Mass Spectrom.* 19, 2497–2506. <https://doi.org/10.1002/rcm.2090>
- 1109 Fuller, B.T., Richards, M.P., Mays, S.A., 2003. Stable carbon and nitrogen isotope variations in
 1110 tooth dentine serial sections from Wharram Percy. *J. Archaeol. Sci.* 30, 1673–1684.
 1111 [https://doi.org/10.1016/S0305-4403\(03\)00073-6](https://doi.org/10.1016/S0305-4403(03)00073-6)
- 1112 Fuller, W.A., 1959. The horns and teeth as indicators of age in bison. *J. Wildl. Manage.* 23, 342–
 1113 344. <https://doi.org/10.2307/3796894>
- 1114 Funck, J., Kellam, C., Seaton, T., Wooller, M.J., 2020. Stable isotopic signatures in modern
 1115 wood bison (*Bison bison athabasca*) hairs as telltale biomarkers of nutritional stress. *Can.*
 1116 *J. Zool.* 98, 505-514. <https://doi.org/10.1139/cjz-2019-0185#XymTQRNKiek>
- 1117 Gadbury, C., Todd, L., Jahren, A.H., Amundson, R., 2000. Spatial and temporal variations in the
 1118 isotopic composition of bison tooth enamel from the Early Holocene Hudson-Meng Bone
 1119 Bed, Nebraska. *Palaeogeogr. Palaeoclimatol. Palaeoecol.* 157, 79–93.
 1120 [https://doi.org/10.1016/S0031-0182\(99\)00151-0](https://doi.org/10.1016/S0031-0182(99)00151-0)
- 1121 Gaglioti, B. V., Mann, D.H., Groves, P., Kunz, M.L., Farquharson, L.M., Reanier, R.E., Jones,
 1122 B.M., Wooller, M.J., 2018. Aeolian stratigraphy describes ice-age paleoenvironments in
 1123 unglaciated Arctic Alaska. *Quat. Sci. Rev.* 182, 175–190.
 1124 <https://doi.org/10.1016/j.quascirev.2018.01.002>
- 1125 Gaglioti, B. V., Mann, D.H., Wooller, M.J., Jones, B.M., Wiles, G.C., Groves, P., Kunz, M.L.,
 1126 Baughman, C.A., Reanier, R.E., 2017. Younger-Dryas cooling and sea-ice feedbacks were
 1127 prominent features of the Pleistocene-Holocene transition in Arctic Alaska. *Quat. Sci. Rev.*
 1128 169, 330–343. <https://doi.org/10.1016/j.quascirev.2017.05.012>
- 1129 Gignoux, C., Grimes, V., Tütken, T., Knecht, R., Britton, K., 2017. Reconstructing caribou
 1130 seasonal biogeography in Little Ice Age (late Holocene) Western Alaska using intra-tooth
 1131 strontium and oxygen isotope analysis. *J. Archaeol. Sci. Reports* 0–1.
 1132 <https://doi.org/10.1016/j.jasrep.2017.10.043>
- 1133 Glassburn, C.L., Potter, B.A., Clark, J.L., Reuther, J.D., Bruning, D.L., Wooller, M.J., 2018.
 1134 Strontium and Oxygen Isotope Profiles of Sequentially Sampled Modern Bison (*Bison*
 1135 *bison bison*) Teeth from Interior Alaska as Proxies of Seasonal Mobility. *Arctic* 71, 185–
 1136 202.

- 1137 Glassburn, C.L., Potter, B.A., Clark, J.L., Reuther, J.D., Bruning, D.L., Wooller, M.J., Clark,
1138 J.L., Reuther, J.D., Bruning, D.L., Wooller, M.J., 2015. Application of strontium and
1139 oxygen isotope analyses to sequentially-sampled modern bison (*Bison bison bison*) teeth
1140 from Interior Alaska as a proxy of seasonal mobility. (Masters Thesis). Univ. Alaska
1141 Fairbanks.
- 1142 Gomes, L., Augusto, W., Godoy, C., 2006. A review of postfeeding larval dispersal in blowflies :
1143 implications for forensic entomology. *Naturwissenschaften* 93, 207–215.
1144 <https://doi.org/10.1007/s00114-006-0082-5>
- 1145 Graham, R.W., Belmecheri, S., Choy, K., Culleton, B.J., Davies, L.J., Froese, D., Heintzman,
1146 P.D., Hritz, C., Kapp, J.D., Newsom, L.A., Rawcliffe, R., Saulnier-Talbot, É., Shapiro, B.,
1147 Wang, Y., Williams, J.W., Wooller, M.J., 2016. Timing and causes of mid-Holocene
1148 mammoth extinction on St. Paul Island, Alaska. *Proc. Natl. Acad. Sci.* 201604903.
1149 <https://doi.org/10.1073/pnas.1604903113>
- 1150 Green, W.C.H., Rothstein, A., Griswold, J.G., 1993. Weaning and Parent-Offspring Conflict:
1151 Variation Relative to Interbirth Interval in Bison. *Ethology* 95, 105-125.
1152 <https://doi.org/10.1111/j.1439-0310.1993.tb00462.x>
- 1153 Guthrie, A.R.D., 1966. Bison Horn Cores : Character Choice and Systematics. *J. Paleontol.* 40,
1154 738–740.
- 1155 Guthrie, R.D., 2001. Origin and causes of the mammoth steppe: A story of cloud cover, woolly
1156 mammal tooth pits, buckles, and inside-out Beringia. *Quat. Sci. Rev.* 20, 549–574.
1157 [https://doi.org/10.1016/S0277-3791\(00\)00099-8](https://doi.org/10.1016/S0277-3791(00)00099-8)
- 1158 Guthrie, R.D., 1989. *Frozen Fauna of Mammoth Steppe: The Story of Blue Babe*. University of
1159 Chicago Press, Chicago.
- 1160 Guthrie, R.D., 1970. Bison Evolution and Zoogeography in North America During the
1161 Pleistocene. *Q. Rev. Biol.* 45, 1–15.
- 1162 Guthrie, R.D., 1968. Paleocology of the Large-Mammal Community in Interior Alaska during
1163 the Late Pleistocene in of the Large-mammal Community. *Am. Midl. Nat.* 79, 346–363.
- 1164 Habran, S., Debier, C., Crocker, D.E., Houser, D.S., Lepoint, G., Bouquegneau, J.M., Das, K.,
1165 2010. Assessment of gestation, lactation and fasting on stable isotope ratios in northern
1166 elephant seals (*Mirounga angustirostris*). *Mar. Mammal Sci.* 26, 880–895.
1167 <https://doi.org/10.1111/j.1748-7692.2010.00372.x>
- 1168 Haile, J., Froese, D.G., Macphee, R.D.E., Roberts, R.G., Arnold, L.J., Reyes, A. V, Rasmussen,
1169 M., Nielsen, R., Brook, B.W., Robinson, S., Demuro, M., Gilbert, M.T.P., Willerslev, E.,
1170 Munch, K., Austin, J.J., Cooper, A., Barnes, I., Mo, P., 2009. Ancient DNA reveals late
1171 survival of mammoth and horse in interior Alaska. *PNAS* 106, 22352–22357.
- 1172 Hanson, J.R., 2015. Bison ecology in the Northern Plains and a reconstruction of bison patterns
1173 for the North Dakota Region. *Plains Anthr.* 29, 93–113.

- 1174 Haynes, G., 1980. Paleontological Society Evidence of Carnivore Gnawing on Pleistocene and
 1175 Recent Mammalian Bones Author (s): Gary Haynes Published by : Paleontological Society
 1176 Stable URL : <https://www.jstor.org/stable/2400350> and Recent mammalian bones.
 1177 Paleobiology 6, 341–351.
- 1178 Heaton, T.H.E., Vogel, J.C., von la Chevallerie, G., Collett, G., 1986. Climatic influence on the
 1179 isotopic composition of bone nitrogen. Nature 322, 822.
 1180 <https://doi.org/https://doi.org/10.1038/322822a0>
- 1181 Hedges, R.E.M., Clement, J.G., Thomas, D.L., O’Connell, T.C., 2007. Collagen Turnover in the
 1182 Adult Femoral Mid-Shaft Modeled from Anthropogenic Radiocarbon Traver
 1183 Measurements. Am. J. Phys. Anthr. 133, 808–816. <https://doi.org/10.1002/ajpa>
- 1184 Hedges, R.E.M., Stevens, R.E., Richards, M.P., 2004. Bone as a stable isotope archive for local
 1185 climatic information. Quat. Sci. Rev. 23, 959–965.
 1186 <https://doi.org/10.1016/j.quascirev.2003.06.022>
- 1187 Heintzman, P.D., Froese, D., Ives, J.W., Soares, A.E.R., Zazula, G.D., Letts, B., Andrews, T.D.,
 1188 Driver, J.C., Hall, E., Gregory Hare, P., Jass, C.N., Mackay, G., Southon, J.R., Stiller, M.,
 1189 Woywitka, R., Suchard, M.A., Shapiro, B., 2016. Bison phylogeography constrains
 1190 dispersal and viability of the Ice Free Corridor in western Canada. PNAS 1–7.
 1191 <https://doi.org/10.1073/pnas.1601077113>
- 1192 Higgins, P., MacFadden, B.J., 2004. “Amount Effect” recorded in oxygen isotopes of Late
 1193 Glacial horse (*Equus*) and bison (*Bison*) teeth from the Sonoran and Chihuahuan deserts,
 1194 southwestern United States. Palaeogeogr. Palaeoclimatol. Palaeoecol. 206, 337–353.
 1195 <https://doi.org/10.1016/j.palaeo.2004.01.011>
- 1196 Hobbie, J.E., Hobbie, E.A., 2006. ¹⁵N in symbiotic fungi and plants estimates nitrogen and
 1197 carbon flux rates in arctic tundra. Ecology 87, 816–822. [https://doi.org/10.1890/0012-9658\(2006\)87\[816:NISFAP\]2.0.CO;2](https://doi.org/10.1890/0012-9658(2006)87[816:NISFAP]2.0.CO;2)
- 1199 Hobson, K.A., Alisauskas, R.A.Y.T., Clark, R.G., 1993. Stable-Nitrogen Isotope Enrichment in
 1200 Avian Tissues Due to Fasting and Nutritional Stress: Implications for Isotopic Analyses of
 1201 Diet. Condor 95, 388–394.
- 1202 Hobson, K.A., Clark, R.G., 1992. Assessing Avian Diets Using Stable Isotopes II : Factors
 1203 Influencing Diet-Tissue Fractionation. Condor 94, 189–197.
- 1204 Hoppe, K. a, Koch, P.L., Carlson, R.W., Webb, S.D., 1999. Tracking mammoths and
 1205 mastodons : Reconstruction of migratory behavior using strontium isotope ratios. Geology
 1206 27, 439–442. [https://doi.org/10.1130/0091-7613\(1999\)027<0439](https://doi.org/10.1130/0091-7613(1999)027<0439)
- 1207 Hoppe, K.A., 2006. Correlation between the oxygen isotope ratio of North American bison teeth
 1208 and local waters: Implication for paleoclimatic reconstructions. Earth Planet. Sci. Lett. 244,
 1209 408–417. <https://doi.org/10.1016/j.epsl.2006.01.062>
- 1210 Hoppe, K.A., 2004. Late Pleistocene mammoth herd structure, migration patterns, and Clovis
 1211 hunting strategies inferred from isotopic analyses of multiple death assemblages.

- 1212 Paleobiology 30, 129–145.
- 1213 Hoppe, K.A., Paytan, A., Chamberlain, P., 2006. Reconstructing grassland vegetation and
1214 paleotemperatures using carbon isotope ratios of bison tooth enamel. *Geology* 34, 649–652.
1215 <https://doi.org/10.1130/G22745.1>
- 1216 Hudson, J., 1993. A Carnivore’s view of archaeological bone assemblages, in: *From Bones to*
1217 *Behavior*. The Center for Archaeological Investigations at Southern Illinois University,
1218 Carbondale, pp. 273–300.
- 1219 Hulten, E., 1968. *Flora of Alaska and Neighboring Territories*. Stanford University Press,
1220 Stanford, California.
- 1221 Iacumin, P., Bocherens, H., Chaix, L., 2001. C and N stable isotope ratios of fossil cattle keratin
1222 horn from Kerma (Sudan): A record of dietary changes. *Ital. J. Int. Sci.* 14, 41–46.
- 1223 Jónsson, H., Ginolhac, A., Schubert, M., Johnson, P.L.F., Orlando, L., 2013. MapDamage2.0:
1224 Fast approximate Bayesian estimates of ancient DNA damage parameters. *Bioinformatics*
1225 29, 1682–1684. <https://doi.org/10.1093/bioinformatics/btt193>
- 1226 Julien, M., Bocherens, H., Burke, A., Drucker, D.G., Patou-mathis, M., Krotova, O., Péan, S.,
1227 2012. Were European steppe bison migratory? $\delta^{18}\text{O}$, $\delta^{13}\text{C}$ and Sr intra-tooth isotopic
1228 variations applied to a palaeoethological reconstruction. *Quat. Int.* 271, 106–119.
1229 <https://doi.org/10.1016/j.quaint.2012.06.011>
- 1230 Kirillova, I. V., Zanina, O.G., Chernova, O.F., Lapteva, E.G., Trofimova, S.S., Lebedev, V.S.,
1231 Tiunov, A. V., Soares, A.E.R., Shidlovskiy, F.K., Shapiro, B., 2015. An ancient bison from
1232 the mouth of the Rauchua River (Chukotka, Russia). *Quat. Res.* 84, 232–245.
1233 <https://doi.org/10.1016/j.yqres.2015.06.003>
- 1234 Knudson, K.J., Williams, S.R., Osborn, R., Forgey, K., Ryan, P., 2009. The geographic origins
1235 of Nasca trophy heads using strontium, oxygen, and carbon isotope data. *J. Anthropol.*
1236 *Archaeol.* 28, 244–257. <https://doi.org/10.1016/j.jaa.2008.10.006>
- 1237 Koch, P.L., Heisinger, J., Moss, C., Carlson, R.W., Marilyn, L., Koch, P.L., Heisinger, J., Moss,
1238 C., Carlson, R.W., Fogel, M.L., Behrensmeyer, A.K., 1995. Isotopic Tracking of Change in
1239 Diet and Habitat Use in African Elephants. *Science* (80-.). 267, 1340–1343.
- 1240 Koch, P.P.L., Tuross, N., Fogel, M.L., 1997. The effects of sample treatment and diagenesis on
1241 the isotopic integrity of carbonate in biogenic hydroxylapatite. *J. Archaeol. Sci.* 24, 417–
1242 429. <https://doi.org/10.1006/jasc.1996.0126>
- 1243 Kootker, L.M., van Lanen, R.J., Kars, H., Davies, G.R., 2016. Strontium isoscapes in The
1244 Netherlands. Spatial variations in $^{87}\text{Sr}/^{86}\text{Sr}$ as a proxy for palaeomobility. *J. Archaeol. Sci.*
1245 *Reports* 6, 1–13. <https://doi.org/10.1016/j.jasrep.2016.01.015>
- 1246 Kowalczyk, R., Taberlet, P., Coissac, E., Valentini, A., Miquel, C., Kamiński, T., Wójcik, J.M.,
1247 2011. Influence of management practices on large herbivore diet-Case of European bison in
1248 Białowieża Primeval Forest (Poland). *For. Ecol. Manage.* 261, 821–828.
1249 <https://doi.org/10.1016/j.foreco.2010.11.026>

- 1250 Kristensen, D.K., Kristensen, E., Forchhammer, M.C., Michelsen, A., Schmidt, N.M., 2011.
 1251 Arctic herbivore diet can be inferred from stable carbon and nitrogen isotopes in C₃ plants,
 1252 faeces, and wool. *Can. J. Zool.* 89, 892–899. <https://doi.org/10.1139/z11-073>
- 1253 Lachniet, M.S., Lawson, D.E., Stephen, H., Sloat, A.R., Patterson, W.P., 2016. Isoscapes of
 1254 d18O and d2H reveal climatic forcings on Alaska and Yukon precipitation. *Water Resour.*
 1255 *Res.* 52, 6575–6586. <https://doi.org/10.1002/2016WR019436>. Received
- 1256 Lambeck, K., Rouby, H., Purcell, A., Sun, Y., Sambridge, M., 2014. Sea level and global ice
 1257 volumes from the Last Glacial Maximum to the Holocene. *Proc. Natl. Acad. Sci. U. S. A.*
 1258 111, 15296–15303. <https://doi.org/10.1073/pnas.1411762111>
- 1259 Larter, N.C., Gates, C.C., 1991. Diet and habitat selection of wood bison in relation to seasonal-
 1260 changes in forage quantity and quality. *Can. J. Zool.* 69, 2677–2685.
 1261 <https://doi.org/10.1139/z91-376>
- 1262 Lee, T.N., Buck, C.L., Barnes, B.M., O'Brien, D.M., 2012. A test of alternative models for
 1263 increased tissue nitrogen isotope ratios during fasting in hibernating arctic ground squirrels.
 1264 *J. Exp. Biol.* 215, 3354–61. <https://doi.org/10.1242/jeb.068528>
- 1265 Li, H., Durbin, R., 2009. Fast and accurate short read alignment with Burrows-Wheeler
 1266 transform. *Bioinformatics* 25, 1754–1760. <https://doi.org/10.1093/bioinformatics/btp324>
- 1267 Lindroth, C.H., 1966. The ground beetles (Carabidae, excl. Cicindellidae) of Canada and Alaska,
 1268 Part 4. *Opusc. Entomol. Suppl.* 29, 409–648.
- 1269 Lisiecki, L.E., Raymo, M.E., 2005. A Pliocene-Pleistocene stack of 57 globally distributed
 1270 benthic δ¹⁸O records. *Paleoceanography* 20, 1–17. <https://doi.org/10.1029/2004PA001071>
- 1271 Lorenzen, E.D., Nogués-Bravo, D., Orlando, L., Weinstock, J., Binladen, J., Marske, K.A.,
 1272 Ugan, A., Borregaard, M.K., Gilbert, M.T.P., Nielsen, R., Ho, S.Y.W., Goebel, T., Graf,
 1273 K.E., Byers, D., Stenderup, J.T., Rasmussen, M., Campos, P.F., Leonard, J.A., Koepfli,
 1274 K.P., Froese, D., Zazula, G., Stafford, T.W., Aris-Sørensen, K., Batra, P., Haywood, A.M.,
 1275 Singarayer, J.S., Valdes, P.J., Boeskorov, G., Burns, J.A., Davydov, S.P., Haile, J., Jenkins,
 1276 D.L., Kosintsev, P., Kuznetsova, T., Lai, X., Martin, L.D., McDonald, H.G., Mol, D.,
 1277 Meldgaard, M., Munch, K., Stephan, E., Sablin, M., Sommer, R.S., Sipko, T., Scott, E.,
 1278 Suchard, M.A., Tikhonov, A., Willerslev, R., Wayne, R.K., Cooper, A., Hofreiter, M., Sher,
 1279 A., Shapiro, B., Rahbek, C., Willerslev, E., 2011. Species-specific responses of Late
 1280 Quaternary megafauna to climate and humans. *Nature* 479, 359–364.
 1281 <https://doi.org/10.1038/nature10574>
- 1282 Lott, D.F., 1971. Sexual and aggressive behavior of American bison (*Bison bison*), in: *The*
 1283 *Behaviour of Ungulates and Its Relation to Management*. pp. 382–394.
- 1284 Lyman, R.L., 1994. *Vertebrate Taphonomy*. Cambridge University Press, Cambridge.
- 1285 Lyman, R.L., 1987. Archaeofaunas and Butchery Studies: A Taphonomic Perspective. *Adv.*
 1286 *Archeol. Method Theory* 10, 249–337.
- 1287 Maher, C.R., Byers, J.A., 1987. Age-related changes in reproductive effort of male bison. *Behav.*

- 1288 Ecol. Sociobiol. 21, 91–96. <https://doi.org/10.1007/PL00020232>
- 1289 Mann, D.H., Groves, P., Kunz, M.L., Reanier, R.E., Gaglioti, B. V., 2013. Ice-age megafauna in
1290 Arctic Alaska: Extinction, invasion, survival. *Quat. Sci. Rev.* 70, 91–108.
1291 <https://doi.org/10.1016/j.quascirev.2013.03.015>
- 1292 Mann, D.H., Groves, P., Reanier, R.E., Gaglioti, B. V, Kunz, M.L., Shapiro, B., 2015. Life and
1293 extinction of megafauna in the ice-age Arctic. *Proc. Natl. Acad. Sci.* 112, 14301–14306.
1294 <https://doi.org/10.1073/pnas.1516573112>
- 1295 Männel, T.T., Auerswald, K., Schnyder, H., 2007. Altitudinal gradients of grassland carbon and
1296 nitrogen isotope composition are recorded in the hair of grazers. *Glob. Ecol. Biogeogr.* 16,
1297 583–592. <https://doi.org/10.1111/j.1466-8238.2007.00322.x>
- 1298 Marcenko, E., Srdoc, D., Golubic, S., Pezdic, J., Head, M.J., 1989. Carbon uptake in aquatic
1299 plants deduced from their natural ¹³C and ¹⁴C content. *Radiocarbon* 31, 785–794.
1300 <https://doi.org/10.1017/S0033822200012406>
- 1301 Marsolier-Kergoat, M.C., Palacio, P., Berthonaud, V., Maksud, F., Stafford, T., Begouen, R.,
1302 Elalouf, J.M., 2015. Hunting the Extinct Steppe Bison (*Bison priscus*) Mitochondrial
1303 Genome in the Trois-Freres Paleolithic Painted Cave. *PLoS One* 10, e0128267.
1304 <https://doi.org/10.1371/journal.pone.0128267>
- 1305 Martin, J.M., Mead, J.I., Barboza, P.S., 2018. Bison body size and climate change. *J. Mammal.*
1306 8, 1–11. <https://doi.org/10.1002/ece3.4019>
- 1307 Mekota, A.-M., Grupe, G., Ufer, S., Cuntz, U., 2006. Serial analysis of stable nitrogen and
1308 carbon isotopes in hair: monitoring starvation and recovery phase of patients suffering from
1309 anorexia nervosa. *Rapid Commun. Mass Spectrom.* 20, 1604–1610.
1310 <https://doi.org/10.1002/rcm>
- 1311 Meyer, H., Schirrmeister, L., Andreev, A., Wagner, D., Hubberten, H.W., Yoshikawa, K.,
1312 Bobrov, A., Wetterich, S., Opel, T., Kandiano, E., Brown, J., 2010. Lateglacial and
1313 Holocene isotopic and environmental history of northern coastal Alaska - Results from a
1314 buried ice-wedge system at Barrow. *Quat. Sci. Rev.* 29, 3720–3735.
1315 <https://doi.org/10.1016/j.quascirev.2010.08.005>
- 1316 Meyer, M., Kircher, M., 2010. Illumina Sequencing Library Preparation for Highly Multiplexed
1317 Target Capture and Sequencing. *Cold Spring Harb. Protoc.*
1318 <https://doi.org/10.1101/pdb.prot5448>
- 1319 Montgomery, J., Evans, J., Horstwood, M.S.A., 2010. Evidence for long-term averaging of
1320 strontium in bovine enamel using TIMS and LA-MC-ICP-MS strontium isotope intra-molar
1321 profiles, *Environmental archeology*. <https://doi.org/10.1063/1.2756072>
- 1322 Moon, T.A., Overeem, I., Druckenmiller, M., Holland, M., Huntington, H., Kling, G., Lovecraft,
1323 A.L., Miller, G., Scambos, T., Schädel, C., Schuur, E.A.G., Trochim, E., Wiese, F.,
1324 Williams, D., Wong, G., 2019. The Expanding Footprint of Rapid Arctic Change. *Earth's*
1325 *Futur.* 7, 212–218. <https://doi.org/10.1029/2018EF001088>

- 1326 Murray, G.G.R., Wang, F., Harrison, E.M., Paterson, G.K., Mather, A.E., Harris, S.R., Holmes,
1327 M.A., Rambaut, A., Welch, J.J., 2016. The effect of genetic structure on molecular dating
1328 and tests for temporal signal. *Methods Ecol. Evol.* 7, 80–89. [https://doi.org/10.1111/2041-](https://doi.org/10.1111/2041-210X.12466)
1329 [210X.12466](https://doi.org/10.1111/2041-210X.12466)
- 1330 Nelson, M.A., Quakenbush, L.T., Mahoney, B.A., Taras, B.D., Wooller, M.J., 2018. Fifty years
1331 of Cook Inlet beluga whale feeding ecology from isotopes in bone and teeth. *Endanger.*
1332 *Species Res.* 36, 77–87. <https://doi.org/10.3354/ESR00890>
- 1333 Paradis, E., Claude, J., Strimmer, K., 2004. APE: Analyses of phylogenetics and evolution in R
1334 language. *Bioinformatics* 20, 289–290. <https://doi.org/10.1093/bioinformatics/btg412>
- 1335 Passey, B.H., Robinson, T.F., Ayliffe, L.K., Cerling, T.E., Sponheimer, M., Dearing, M.D.,
1336 Roeder, B.L., Ehleringer, J.R., 2005. Carbon isotope fractionation between diet, breath CO₂,
1337 and bioapatite in different mammals. *J. Archaeol. Sci.* 32, 1459–1470.
1338 <https://doi.org/10.1016/j.jas.2005.03.015>
- 1339 Pellegrini, M., Donahue, R.E., Chenery, C., Evans, J., Lee-Thorp, J., Montgomery, J., Mussi, M.,
1340 2008. Faunal migration in late-glacial central Italy: Implications for human resource
1341 exploitation. *Rapid Commun. Mass Spectrom.* 22, 1714–1726.
1342 <https://doi.org/10.1002/rcm.3521>
- 1343 Pellegrini, M., Snoeck, C., 2016. Comparing bioapatite carbonate pre-treatments for isotopic
1344 measurements: Part 2 - Impact on carbon and oxygen isotope compositions. *Chem. Geol.*
1345 420, 88–96. <https://doi.org/10.1016/j.chemgeo.2015.10.038>
- 1346 Plumb, G.E., White, P.J., Coughenour, M.B., Wallen, R.L., 2009. Carrying capacity, migration,
1347 and dispersal in Yellowstone bison. *Biol. Conserv.* 142, 2377–2387.
1348 <https://doi.org/10.1016/j.biocon.2009.05.019>
- 1349 Post, D.M., 2002. Using Stable Isotopes to Estimate Trophic Position: Models, Methods and
1350 Assumptions. *Ecology* 83, 703–718.
- 1351 Post, E., Forchhammer, M.C., 2008. Climate change reduces reproductive success of an Arctic
1352 herbivore through trophic mismatch. *Philos. Trans. R. Soc. B Biol. Sci.* 363, 2369–2375.
1353 <https://doi.org/10.1098/rstb.2007.2207>
- 1354 Rabanus-Wallace, M.T., Wooller, M.J., Zazula, G.D., Shute, E., Jahren, A.H., Kosintsev, P.,
1355 Burns, J.A., Breen, J., Llamas, B., Cooper, A., 2017. Megafaunal isotopes reveal role of
1356 increased moisture on rangeland during late Pleistocene extinctions. *Nat. Ecol. Evol.* 1, 1–5.
1357 <https://doi.org/10.1038/s41559-017-0125>
- 1358 Radloff, F.G.T., Mucina, L., Bond, W.J., le Roux, P.J., 2010. Strontium isotope analyses of large
1359 herbivore habitat use in the Cape Fynbos region of South Africa. *Oecologia* 164, 567–578.
1360 <https://doi.org/10.1007/s00442-010-1731-0>
- 1361 Rasmussen, S.O., Bigler, M., Blockley, S.P., Blunier, T., Buchardt, S.L., Clausen, H.B.,
1362 Cvijanovic, I., Dahl-Jensen, D., Johnsen, S.J., Fischer, H., Gkinis, V., Guillevic, M., Hoek,
1363 W.Z., Lowe, J.J., Pedro, J.B., Popp, T., Seierstad, I.K., Steffensen, J.P., Svensson, A.M.,

- 1364 Vallelonga, P., Vinther, B.M., Walker, M.J.C., Wheatley, J.J., Winstrup, M., 2014. A
 1365 stratigraphic framework for abrupt climatic changes during the Last Glacial period based on
 1366 three synchronized Greenland ice-core records: Refining and extending the INTIMATE
 1367 event stratigraphy. *Quat. Sci. Rev.* 106, 14–28.
 1368 <https://doi.org/10.1016/j.quascirev.2014.09.007>
- 1369 Reitsema, L.J., Muir, A.B., 2015. Brief communication: Growth velocity and weaning $\delta^{15}\text{N}$
 1370 “dips” during ontogeny in *Macaca mulatta*. *Am. J. Phys. Anthropol.* 157, 347–357.
 1371 <https://doi.org/10.1002/ajpa.22713>
- 1372 Rivals, F., Mithlacher, M.C., Solounias, N., Mol, D., Semprebon, G.M., de Vos, J., Kalthoff,
 1373 D.C., 2010. Palaeoecology of the Mammoth Steppe fauna from the late Pleistocene of the
 1374 North Sea and Alaska: Separating species preferences from geographic influence in
 1375 paleoecological dental wear analysis. *Palaeogeogr. Palaeoclimatol. Palaeoecol.* 286, 42–54.
 1376 <https://doi.org/10.1016/j.palaeo.2009.12.002>
- 1377 Rivals, F., Solounias, N., Mithlacher, M.C., 2007. Evidence for geographic variation in the diets
 1378 of late Pleistocene and early Holocene Bison in North America, and differences from the
 1379 diets of recent Bison. *Quat. Res.* 68, 338–346. <https://doi.org/10.1016/j.yqres.2007.07.012>
- 1380 Rode, K.D., Stricker, C.A., Erlenbach, J., Robbins, C.T., Cherry, S.G., Newsome, S.D., Cutting,
 1381 A., Jensen, S., Stenhouse, G., Brooks, M., Hash, A., Nicassio, N., 2016. Isotopic
 1382 Incorporation and the Effects of Fasting and Dietary Lipid Content on Isotopic
 1383 Discrimination in Large Carnivorous Mammals. *Physiol. Biochem. Zool.* 89, 182–197.
 1384 <https://doi.org/10.1086/686490>
- 1385 Rode, K.D., Wilson, R.R., Douglas, D.C., Muhlenbruch, V., Atwood, T.C., Regehr, E. V.,
 1386 Richardson, E.S., Pilfold, N.W., Derocher, A.E., Durner, G.M., Stirling, I., Amstrup, S.C.,
 1387 St. Martin, M., Pagano, A.M., Simac, K., 2018. Spring fasting behavior in a marine apex
 1388 predator provides an index of ecosystem productivity. *Glob. Chang. Biol.* 24, 410–423.
 1389 <https://doi.org/10.1111/gcb.13933>
- 1390 Saarinen, J.J., Eronen, J.T., Fortelius, M., Seppä, H., Lister, A., 2016. Patterns of body mass and
 1391 diet of large ungulates from Middle and Late Pleistocene of Western Europe and their
 1392 connections with vegetation openness. *Paleontol. Electron.* 1–58.
- 1393 Scherler, L., Tütken, T., Becker, D., 2014. Carbon and oxygen stable isotope compositions of
 1394 late Pleistocene mammal teeth from dolines of Ajoie (Northwestern Switzerland). *Quat.*
 1395 *Res.* 82, 378–387. <https://doi.org/10.1016/j.yqres.2014.05.004>
- 1396 Schmieder, R., Edwards, R., 2011. Quality control and preprocessing of metagenomic datasets.
 1397 *Bioinformatics* 27, 863–864. <https://doi.org/10.1093/bioinformatics/btr026>
- 1398 Schoeninger, M.J., DeNiro, M.J., 1984. Nitrogen and carbon isotopic composition of bone
 1399 collagen from marine and terrestrial animals. *Geochim. Cosmochim. Acta* 48, 625–639.
 1400 [https://doi.org/10.1016/0016-7037\(84\)90091-7](https://doi.org/10.1016/0016-7037(84)90091-7)
- 1401 Schubert, B.W., 2010. Late Quaternary chronology and extinction of North American giant
 1402 short-faced bears (*Arctodus simus*). *Quat. Int.* 217, 188–194.

- 1403 <https://doi.org/10.1016/j.quaint.2009.11.010>
- 1404 Schwartz-Narbonnea, R., Longstaffea, F.J., Kardynalb, K.J., Druckenmiller, P., Hobson, K.A.
1405 Jasse, C.N., Metcalfe, J.Z., Zazula, J.Z. 2019. Reframing the mammoth steppe: Insights
1406 from analysis of isotopic niches. *Quat. Sci. Rev.* 215, 1-21.
1407 <https://doi.org/10.1016/j.quascirev.2019.04.025>
- 1408 Shapiro, B., Cooper, A., 2003. Beringia as an Ice Age genetic museum. *Quat. Res.* 60, 94–100.
1409 [https://doi.org/10.1016/S0033-5894\(03\)00009-7](https://doi.org/10.1016/S0033-5894(03)00009-7)
- 1410 Shapiro, B., Ho, S.Y.W., Drummond, A.J., Suchard, M.A., Pybus, O.G., Rambaut, A., 2011. A
1411 bayesian phylogenetic method to estimate unknown sequence ages. *Mol. Biol. Evol.* 28,
1412 879–887. <https://doi.org/10.1093/molbev/msq262>
- 1413 Shapiro, B., Pybus, O.G., Gilbert, M.T.P., Barnes, I., Baryshnikov, G.F., Burns, J.A., Davydov,
1414 S., 2004. Rise and Fall of the Beringian Steppe Bison. *Science* (80-.). 306, 1561–1565.
1415 <https://doi.org/10.1126/science.1101074>
- 1416 Sharma, S., Couturier, S., Côté, S.D., 2009. Impacts of climate change on the seasonal
1417 distribution of migratory caribou. *Glob. Chang. Biol.* 15, 2549–2562.
1418 <https://doi.org/10.1111/j.1365-2486.2009.01945.x>
- 1419 Smith, K.G.V., 1986. *A Manual of Forensic Entomology*. Trustees of the British Museum,
1420 Oxford.
- 1421 Soper, J.D., 1941. History, Range and Home Life of the Northern Bison. *Ecol. Monogr.* 11, 347–
1422 412. <https://doi.org/10.2307/1943298>
- 1423 Sorkin, B., 2006. Ecomorphology of the giant short-faced bears *Agriotherium* and *Arctodus*.
1424 *Hist. Biol.* 18, 1–20. <https://doi.org/10.1080/08912960500476366>
- 1425 Stevens, R.E., Balasse, M., O’Connell, T.C., 2011. Intra-tooth oxygen isotope variation in a
1426 known population of red deer: Implications for past climate and seasonality reconstructions.
1427 *Palaeogeogr. Palaeoclimatol. Palaeoecol.* 301, 64–74.
1428 <https://doi.org/10.1016/j.palaeo.2010.12.021>
- 1429 Stevens, R.E., Hedges, R.E., 2004. Carbon and nitrogen stable isotope analysis of northwest
1430 European horse bone and tooth collagen, 40,000BP–present: Palaeoclimatic interpretations.
1431 *Quat. Sci. Rev.* 23, 977–991. <https://doi.org/10.1016/j.quascirev.2003.06.024>
- 1432 Stevens, R.E., Lister, M., Hedges, R.E.M., 2006. Predicting diet, trophic level and paleoecology
1433 from bone stable isotope analysis: a comparative study of five red deer populations.
1434 *Oecologia* 149, 12–21. <https://doi.org/10.1007/s00442-006-0416-1>
- 1435 Stuiver, M., Reimer, P.J., Reimer, R.W., 2019. CALIB 7.1.
- 1436 Taylor, R.E., Hare, P.E., Prior, C.A., Kirner, D.L., Want, L., Burkyi, R.R., 1995. Radiocarbon
1437 dating of biochemically characterized hair. *Radiocarbon* 37, 319–330.
1438 <https://doi.org/10.1017/S0033822200030794>

- 1439 Van Geel, B., Protopopov, A., Bull, I., Duijm, E., Gill, F., Lammers, Y., Nieman, A., Rudaya,
1440 N., Trofimova, S., Tikhonov, A.N., Vos, R., Zhilich, S., Gravendeel, B., 2014. Multiproxy
1441 diet analysis of the last meal of an early Holocene Yakutian bison. *J. Quat. Sci.* 29, 261–
1442 268. <https://doi.org/10.1002/jqs.2698>
- 1443 Velivetskaya, T.A., Smirnov, N.G., Kiyashko, S.I., Ignatiev, A. V., Ulitko, A.I., 2016.
1444 Resolution-enhanced stable isotope profiles within the complete tooth rows of Late
1445 Pleistocene bisons (Middle Urals, Russia) as a record of their individual development and
1446 environmental changes. *Quat. Int.* 400, 212–226.
1447 <https://doi.org/10.1016/j.quaint.2014.12.011>
- 1448 Verkouteren, R.M., Klinedinst, D.B., 2004. Value Assignment and Uncertainty Estimation of
1449 Selected Light Stable Isotope Reference Materials: RMs 8543-8545, RMs 8562-8564, and
1450 RM 8566, National Institute of Standards and Technology Special Publication.
- 1451 Viner, S., Evans, J., Albarella, U., Parker Pearson, M., 2010. Cattle mobility in prehistoric
1452 Britain: Strontium isotope analysis of cattle teeth from Durrington Walls (Wiltshire,
1453 Britain). *J. Archaeol. Sci.* 37, 2812–2820. <https://doi.org/10.1016/j.jas.2010.06.017>
- 1454 Voigt, C.C., Matt, F., 2004. Nitrogen stress causes unpredictable enrichments of ^{15}N in two
1455 nectar-feeding bat species. *J. Exp. Biol.* 207, 1741–1748. <https://doi.org/10.1242/jeb.00929>
- 1456 Waggoner, V., Hinkes, M., 1986. Summer and Fall Browse Utilization by an Alaskan Bison
1457 Herd. *J. Wildl. Manag.* 50, 322–324.
- 1458 Warren, J., Anderson, G.S., 2013. The development of *Protophormia terraenovae* (Robineau-
1459 Desvoidy) at constant temperatures and its minimum temperature threshold. *Forensic Sci.*
1460 *Int.* 233, 374–379. <https://doi.org/10.1016/j.forsciint.2013.10.012>
- 1461 Widga, C., Walker, J.D., Stockli, L.D., 2010. Middle Holocene Bison diet and mobility in the
1462 eastern Great Plains (USA) based on ^{13}C , ^{18}O , and $^{87}\text{Sr}/^{86}\text{Sr}$ analyses of tooth enamel
1463 carbonate. *Quat. Res.* 73, 449–463. <https://doi.org/10.1016/j.yqres.2009.12.001>
- 1464 Wiener, D.J., Wiedemar, N., Welle, M.M., Drögemüller, C., 2015. Novel features of the prenatal
1465 horn bud development in cattle (*Bos taurus*). *PLoS One* 10, 1–13.
1466 <https://doi.org/10.1371/journal.pone.0127691>
- 1467 Willerslev, E., Davison, J., Moora, M., Zobel, M., Coissac, E., Edwards, M.E., Lorenzen, E.D.,
1468 Vestergård, M., Gussarova, G., Haile, J., Craine, J., Gielly, L., Boessenkool, S., Epp, L.S.,
1469 Pearman, P.B., Cheddadi, R., Murray, D., Bråthen, K.A., Yoccoz, N., Binney, H., Cruaud,
1470 C., Wincker, P., Goslar, T., Alsos, I.G., Bellemain, E., Brysting, A.K., Elven, R., Sønstebø,
1471 J.H., Murton, J., Sher, A., Rasmussen, M., Rønn, R., Mourier, T., Cooper, A., Austin, J.,
1472 Möller, P., Froese, D., Zazula, G., Pompanon, F., Rioux, D., Niderkorn, V., Tikhonov, A.,
1473 Savvinov, G., Roberts, R.G., Macphee, R.D.E., Gilbert, M.T.P., Kjær, K.H., Orlando, L.,
1474 Brochmann, C., Taberlet, P., 2014. Fifty thousand years of Arctic vegetation and
1475 megafaunal diet. *Nature* 506, 47–51. <https://doi.org/10.1038/nature12921>
- 1476 Wooller, M.J., Zazula, G.D., Edwards, M., Froese, D.G., Boone, R.D., Parker, C., Bennett, B.,
1477 2007. Stable carbon isotope compositions of Eastern Beringian grasses and sedges:

- 1478 Investigating their potential as paleoenvironmental indicators. *Arct. Antarct. Alp. Res.* 39,
1479 318–331. [https://doi.org/10.1657/1523-0430\(2007\)39\[318:SCICOE\]2.0.CO;2](https://doi.org/10.1657/1523-0430(2007)39[318:SCICOE]2.0.CO;2)
- 1480 Zazula, G.D., Hall, E., Hare, P.G., Thomas, C., Mathewes, R., La Farge, C., Martel, A.L.,
1481 Heintzman, P.D., Shapiro, B., 2017. A middle holocene steppe bison and
1482 paleoenvironments from the Versleuce Meadows, Whitehorse, Yukon, Canada. *Can. J.*
1483 *Earth Sci.* 54, 1138–1152. <https://doi.org/10.1139/cjes-2017-0100>
- 1484 Zazula, G.D., MacKay, G., Andrews, T.D., Shapiro, B., Letts, B., Brock, F., 2009a. A late
1485 Pleistocene steppe bison (*Bison priscus*) partial carcass from Tsiigehtchic, Northwest
1486 Territories, Canada. *Quat. Sci. Rev.* 28, 2734–2742.
1487 <https://doi.org/10.1016/j.quascirev.2009.06.012>
- 1488 Zazzo, A., Bendrey, R., Vella, D., Moloney, A.P., Monahan, F.J., Schmidt, O., 2012. A refined
1489 sampling strategy for intra-tooth stable isotope analysis of mammalian enamel. *Geochim.*
1490 *Cosmochim. Acta* 84, 1–13. <https://doi.org/10.1016/j.gca.2012.01.012>
- 1491 Zimov, A.S.A., Chuprynin, V.I., Oreshko, A.P., Iii, F.S.C., Reynolds, J.F., 2011. Steppe-Tundra
1492 Transition : A Herbivore-Driven Biome Shift at the End of the Pleistocene. *Am. Soc. Nat.*
1493 146, 765–794. <https://doi.org/10.1086/285824>
- 1494 Zimov, S.A., Zimov, N.S., Tikhonov, A.N., Chapin, I.S., 2012. Mammoth steppe: A high-
1495 productivity phenomenon. *Quat. Sci. Rev.* 57, 26–45.
1496 <https://doi.org/10.1016/j.quascirev.2012.10.005>

1497

1498 **Figure titles:**

1499

1500 Figure 1. a) A map on northern Alaska, with the provenance of steppe bison (*Bison priscus*)
1501 specimen UAMES 29458 indicated by the red star. Yellow dots show rodent specimen localities
1502 and strontium isotope ratios measured from their teeth. The underlying map is modified from
1503 Bataille et al. (2016). b) UAMES 29458 skull in situ during excavation. c) UAMES 29458
1504 articulated thoracic vertebrae attached with connective tissue, in situ during excavation.

1505

1506 Figure 2. a) Specimen UAMES 29458 rearticulated for taphonomic analysis. b) Skeletal
1507 elements missing from specimen are indicated in gray and elements with carnivore marks
1508 indicated in red. All elements from the right side were present.

1509

1510 Figure 3. Scavenger dentition marks on the a) thoracic vertebral processes of *Bison priscus*
1511 specimen UAMES 29458 with bites indicated by arrows, and b) ventral side of lumbar vertebrae
1512 with gnaw marks indicated by arrow c) Vertebrae with healed pathology indicated by arrow.

1513
1514 Figure 4. The macrofossil assemblage taken from skull of specimen UAMES 29458:
1515 *Protophormia terraenovae* puparium UAMES 52319. a), dorsal view b), lateral view c), ventral
1516 view d), posterior view, the posterior spiracles surrounded by a rectangle e), the posterior
1517 spiracles in close-up view. (photos: J.-B. Huchet, 2018), f) Partial abdomen sternites of a ground
1518 beetle UAMES 52334 (Carabidae: Pterostichinae) (photo: J.-B. Huchet, 2018), g) Psyllid
1519 forewing recovered from inside the bison skull UAMES 52331 (photo: J.-B. Huchet, 2018), h)
1520 Right elytron of a ripicolous ground beetle of the genus *Elaphrus* Fabricius UAMES 52333
1521 (Carabidae: Elaphrinae) (photo: J.-B. Huchet, 2018), i) *Carex* seed lenticular, j) *Carex* seed
1522 Trigonal, k) Poaceae caryopsis, l) *Polygonum bistorta*, m) *Draba*-type seed, n) *Andromeda*
1523 *polifolia*, o) *Bryophyta* sp.

1524
1525 Figure 5. The relative abundance of plant macrofossil specimens in the skull and spine of
1526 specimen UAMES 29458, categorized by characteristic eco-type.

1527
1528 Figure 6. Carbon and nitrogen stable isotope values of serial horn sheath samples (n=113) with
1529 dotted trend-line of weighted moving averaging of the nearest 3 samples and collagen carbon and
1530 nitrogen stable isotope values. * Indicate lowest $\delta^{15}\text{N}$ values associated with summer. Labels on
1531 the bottom indicate approximate timing of identifiable life events.

1532
1533 Figure 7. Isotope data from analyses of molar 1 (M1), molar 2 (M2), and molar 3 (M3) from
1534 specimen UAMES 29458. a) Strontium $^{87}\text{Sr}/^{86}\text{Sr}$ ratios, b) Oxygen stable isotope ratios
1535 expressed as $\delta^{18}\text{O}$ values and c) Stable carbon isotope ratios (expressed as $\delta^{13}\text{C}$ values). Shading
1536 represents estimates of winter, based on the $\delta^{18}\text{O}$ values. * Indicate highest $\delta^{18}\text{O}$ values
1537 associated with summer.

1538

1539 Figure 8. Rodent $^{87}\text{Sr}/^{86}\text{Sr}$ ratios grouped by region, compared to $^{87}\text{Sr}/^{86}\text{Sr}$ ratios from specimen
1540 UAMES 29458 over time and a model-predicted $^{87}\text{Sr}/^{86}\text{Sr}$ ratio for the death location of
1541 specimen UAMES 29458.

1542

1543 Figure 9. A Bayesian time-calibrated genealogy of bison mitochondrial genomes, with major
1544 well-supported Clades (1, 1A, 2, 2A, 2B) highlighted (following Heintzman et al., 2016 and
1545 Zazula et al., 2017). All living bison fall within Clade 1A, whereas the specimen UAMES 29458
1546 falls near the base of Clade 2. Purple bars are 95% highest posterior density intervals for node
1547 heights and are shown for nodes with posterior probability >0.95 . This maximum clade
1548 credibility tree resulted from the analysis that excluded MS022 and had a minimum age prior of
1549 30 kya BP for UAMES 29458. Results from the other analyses can be found in Table 6. The
1550 diverged yak tips have been removed.

1551 Figure 10. Comparison of the ranges (Δ) of $^{87}\text{Sr}/^{86}\text{Sr}$ ratios recorded within the teeth of different
1552 bison including, present-day plains bison (*Bison bison*) from interior Alaska (Glassburn et al.,
1553 2018); Holocene plains bison (*Bison bison*) from the American Plains (Widga et al., 2010); Late
1554 Pleistocene steppe bison (*Bison priscus*) from Ukraine (Julien et al., 2012) and Late Pleistocene
1555 steppe bison (*Bison priscus*) from France (Britton et al., 2011).

1556 Figure 11. Summary of all radiocarbon dates (^{14}C), molecular clock estimates, and compatible
1557 $\delta^{18}\text{O}$ value periods based on Greenland Ice core values (Rasmussen et al., 2014) and a $\Delta 4\%$
1558 lower values than present. *dates are calibrated radiocarbon dates where possible, otherwise they
1559 are before present.

1560 **Supplementary materials**

1561 Figure S1. Intra tooth sampling of molar 1 (M1), molar 2 (M2) and molar 3 (M3) from *Bison*
1562 *priscus* specimen UAMES 29458, number indicates sample number.

1563

1564 Figure S2. Serial sampling scheme for bison horn sheath from *Bison priscus* specimen UAMES
1565 29458.

1566

1567 Figure S3. Results of the tests for temporal signal in the bison mitochondrial genome data set. a)
1568 Full alignment data set, and b) reduced alignment data set (excluding MS022). Left panels: linear
1569 regression of phylogenetic root-to-tip distance against sampling date. Center panels: similar-date
1570 clusters (rounded to the nearest thousand years). Right panels: testing the results against random
1571 permutations over the clusters presented in b).

1572

1573 Figure S4. Assessment of damage patterns in nuclear (A-C) and mitochondrial (D-F) DNA
1574 fragments from *Bison priscus* specimen UAMES 29458. (A, D) DNA fragment length
1575 distributions, with means of 90 bp (nuclear) and 127 bp (mitochondrial). (B, E) The relative
1576 frequency of cytosine to thymine deamination (red line) and observed guanine to adenine
1577 misincorporation (blue line) from cytosine deamination on the opposite DNA strand.
1578 Deamination is more prevalent at the ends of ancient DNA fragments. (C, F) DNA fragmentation
1579 plots showing an elevated occurrence of purines (guanine, adenine) immediately upstream of the
1580 ancient DNA fragment (to the left of the grey box) and the opposite signal immediately
1581 downstream of the fragment (to the right of the grey box).

1 Tables**2** Table 1. Summary of radiocarbon dates.

Material	¹⁴C yrs	Error	Cal yr BP CALIB	Laboratory	Accession Number
Collagen	>43,500	NA		BETA	324600
Keratin	46,000	1100	46,962	Keck	209861
Chitin	46,800	1200		Keck	209862
Plant	>49,990	NA		Keck	209863

3 Table 2. Results of isotopic analysis of strontium, carbon and oxygen of UAMES specimen
 4 29458.

Tooth	Sample #	Distance from base of enamel (cm)	$^{87}\text{Sr}/^{86}\text{Sr}$	$\delta^{13}\text{C}$ ‰ (VPDB)	$\delta^{13}\text{C}$ ‰ Std dev	$\delta^{18}\text{O}$ ‰ (VPDB)	$\delta^{18}\text{O}$ ‰ Std dev
M1	1	1.8	0.71117	-11.4	0.1	-19.0	0.1
	2	1.7	0.71087	-11.5	0.3	-20.2	0.3
	3	2.55	0.71116	No data	No data	No data	No data
	4	1.3	0.71132	-11.3	0.4	-21.0	0.5
	5	1.15	0.71125	-11.4	0.5	-23.8	0.9
	6	1	0.71138	-11.0	0.2	-21.0	0.2
	7	0.8	0.71144	-11.2	0.3	-22.1	0.4
	8	0.65	0.71158	-11.3	0.1	-22.2	0.2
	9	0.5	0.71162	-11.2	0.1	-22.2	0.2
	10	0.3	0.71172	-11.7	0.4	-23.2	0.4
	11	0.2	0.71182	-11.4	0.2	-22.1	0.3
M2	1	2.1	0.71172	-10.7	0.1	-18.8	0.3
	2	1.95	0.71184	-10.9	0.2	-19.7	0.6
	3	1.8	0.71198	-11.0	0.1	-19.6	0.1
	4	1.65	0.712	-11.5	0.3	-22.7	0.4
	5	1.45	0.71189	-10.7	0.2	-20.2	0.4
	6	1.35	0.71191	-10.9	0.2	-20.5	0.5
	7	1.1	0.71195	-11.4	0.2	-21.7	0.3
	8	0.95	0.71195	-11.5	0.5	-26.5	0.9
	9	0.75	0.71214	-11.3	0.1	-21.2	0.3
	10	0.6	0.71242	-11.4	0.1	-21.5	0.3
	11	0.45	0.71236	No data	No data	No data	No data
	12	0.3	0.71255	No data	No data	No data	No data
M3	1	2.25	0.71297	-10.9	0.1	-22.3	0.3
	2	2.05	0.71324	-10.5	0.1	-21.0	0.1
	3	1.8	0.71315	-10.5	0.4	-21.0	0.1
	4	1.60	0.71314	-10.9	0.2	-22.3	0.2
	5	1.4	0.71307	-10.5	0.2	-21.1	0.3
	6	1.2	0.71302	-10.3	0.1	-19.7	0.1
	7	1	0.71303	-10.4	0.2	-20.0	0.2
	8	0.85	0.71298	-10.4	0.2	-20.0	0.2
	9	0.6	0.71303	-10.4	0.1	-18.4	0.2
	10	0.45	0.71304	-10.6	0.2	-20.0	0.2

5 Table 3. Rodents use for characterizing $^{87}\text{Sr}/^{86}\text{Sr}$ isoscape.

UAM:						
Mamm	Species	Locality	Environment	Lat	Long	$^{87}\text{Sr}/^{86}\text{Sr}$
4650	<i>Microtus oeconomus</i>	Meade River village	Coastal Plain	70.481	-157.417	0.71007
8163	<i>Microtus oeconomus</i>	Umiat region	Coastal Plain	69.367	-152.133	0.71309
11149	<i>Microtus oeconomus</i>	Kikitaliorak Lake	Mountain Drainage	68.125	-156.233	0.71721
11166	<i>Microtus oeconomus</i>	Feniak Lake	Mountain Lake	68.250	-158.333	0.71372
13614	<i>Microtus oeconomus</i>	Barrow, NARL	Coastal Plain	71.283	-156.783	0.70940
56327	<i>Microtus oeconomus</i>	Desperation Lake	Mountain Lake	68.338	-158.728	0.70619
66866	<i>Microtus miurus</i>	May Lake	Foot Hills	68.617	-153.000	0.71274
78833	<i>Microtus miurus</i>	Agiak Lake	Mountain Lake	68.078	-152.924	0.71502
79046	<i>Microtus miurus</i>	Nanushuk River	Mountain River	68.275	-150.655	0.71695
79102	<i>Microtus oeconomus</i>	Agiak Lake	Mountain Lake	68.081	-152.944	0.71661
82113	<i>Microtus oeconomus</i>	Lake Tulilik	Mountain Lake	68.117	-154.120	0.72047
125703	<i>Microtus oeconomus</i>	Colville River	Foot Hills	69.007	-158.268	0.71107
125706	<i>Dicrostonyx groenlandicus</i>	Colville River	Foot Hills	68.899	-156.470	0.71494
125713	<i>Microtus oeconomus</i>	Colville River	Foot Hills	69.060	-154.244	0.71312

6

7 Table 4. Summary of isotopic results ($\delta^{13}\text{C}$ and $\delta^{18}\text{O}$ reported here vs. VPDB in ‰).

	Mean	Max	Min	Range
$^{87}\text{Sr}/^{86}\text{Sr}$	0.71214	0.71324	0.71087	0.00237
$\delta^{13}\text{C}$	-11.0	-10.3	-11.7	1.5
$\delta^{18}\text{O}$	-21.2	-18.4	-26.5	8.1

8 Table 5. Results of the genomic sex determination analysis. X:A ratio is the ratio of the relative
9 mapping frequency of the X chromosome to that of an autosome (1-29, all). Chr.: chromosome.
10 The minimum and maximum X:A ratios are highlighted in bold.

Chr.	Length	Reads mapped	X:A ratio	Chr.	Length	Reads mapped	X:A ratio
1	161428367	10474	0.543	17	76280064	4915	0.547
2	141965563	9334	0.536	18	65811054	4640	0.500
3	126844711	8357	0.535	19	64845320	4500	0.508
4	123809850	8237	0.530	20	75686341	4995	0.534
5	125249322	8237	0.536	21	69078422	4622	0.527
6	122519025	8008	0.539	22	61598339	4384	0.495
7	113029157	7598	0.525	23	52334015	3652	0.505
8	116846264	7802	0.528	24	64508398	4447	0.511
9	108503706	6828	0.560	25	44081797	3137	0.495
10	105982576	7023	0.532	26	51826547	3480	0.525
11	109987751	7605	0.510	27	48460478	3046	0.561
12	85119472	5420	0.554	28	45964680	3144	0.516
13	84213851	6029	0.493	29	51812796	3432	0.532
14	81216349	5748	0.498	all	2541187220	169841	0.528
15	84472747	5548	0.537				
16	77710258	5199	0.527	X	88654062	3126	NA

11 Table 6. Summary of the Bayesian molecular analyses of JK319/UAMES 29458, with overall
 12 maximum age ranges highlighted in bold

Analysis variables		Phylogenetic placement		Estimated age		
Min. age prior	MS022	Placement	Posterior probability	Minimum	Maximum	ESS
0	Included	1	0.276	32,653	85,157	11376
0	Excluded	1	0.410	36,022	86,643	20465
20,000	Included	1	0.261	34,300	85,618	15546
20,000	Excluded	1	0.409	34,929	85,827	18525
30,000	Included	1	0.268	34,708	83,346	19814
30,000	Excluded	1	0.407	36,696	85,376	18945
40,000	Included	1	0.241	40,021	81,074	19367
40,000	Excluded	1	0.391	40,227	82,423	19013
50,000	Included	2	0.678	50,000	82,285	20687
50,000	Excluded	2	1.000	50,007	82,935	18967

13 Phylogenetic placements are: 1) sister to MS002, and 2) at the base of Clade 2 (see Figure 9).

14 Minimum and maximum ages are based on 95% highest posterior density credibility intervals.

15 Note that, for analyses with a minimum age prior of 40 and 50 kya BP, the estimated minimum

16 ages are likely to have been truncated by the prior. ESS: estimated sample size.

Table 7. Comparison to other Bison strontium data. See Figure 10 *Stratigraphically determined to be from MIS4 **Molecular clock.

Context	Species	N	Date	Average Range	Citation
Present-day					
Interior Alaska	<i>Bison bison</i>	3	2014	0.00111	Glassburn et al. 2018
Holocene					
American					
Plaines	<i>Bison bison</i>	12	8930-6980 cal yr BP	0.00077	Widga et al. 2010
Late Pleistocene					
Ukraine	<i>Bison priscus</i>	24	20557-20,491 cal yr BP	0.00016	Julien et al. 2012
Late Pleistocene					
France	<i>Bison priscus</i>	1	49,000±5 yr BP*	0.00010	Britton et al. 2011
Bison Bob	<i>Bison priscus</i>	1	33-87,000 yr BP**	0.00237	This paper

Figure 1

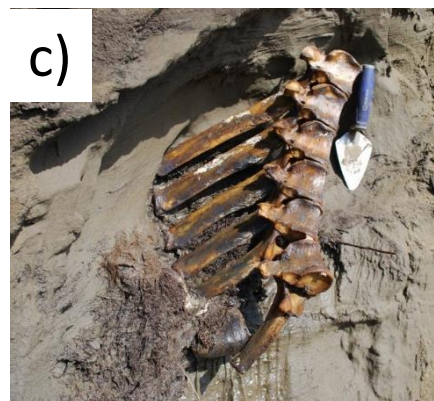
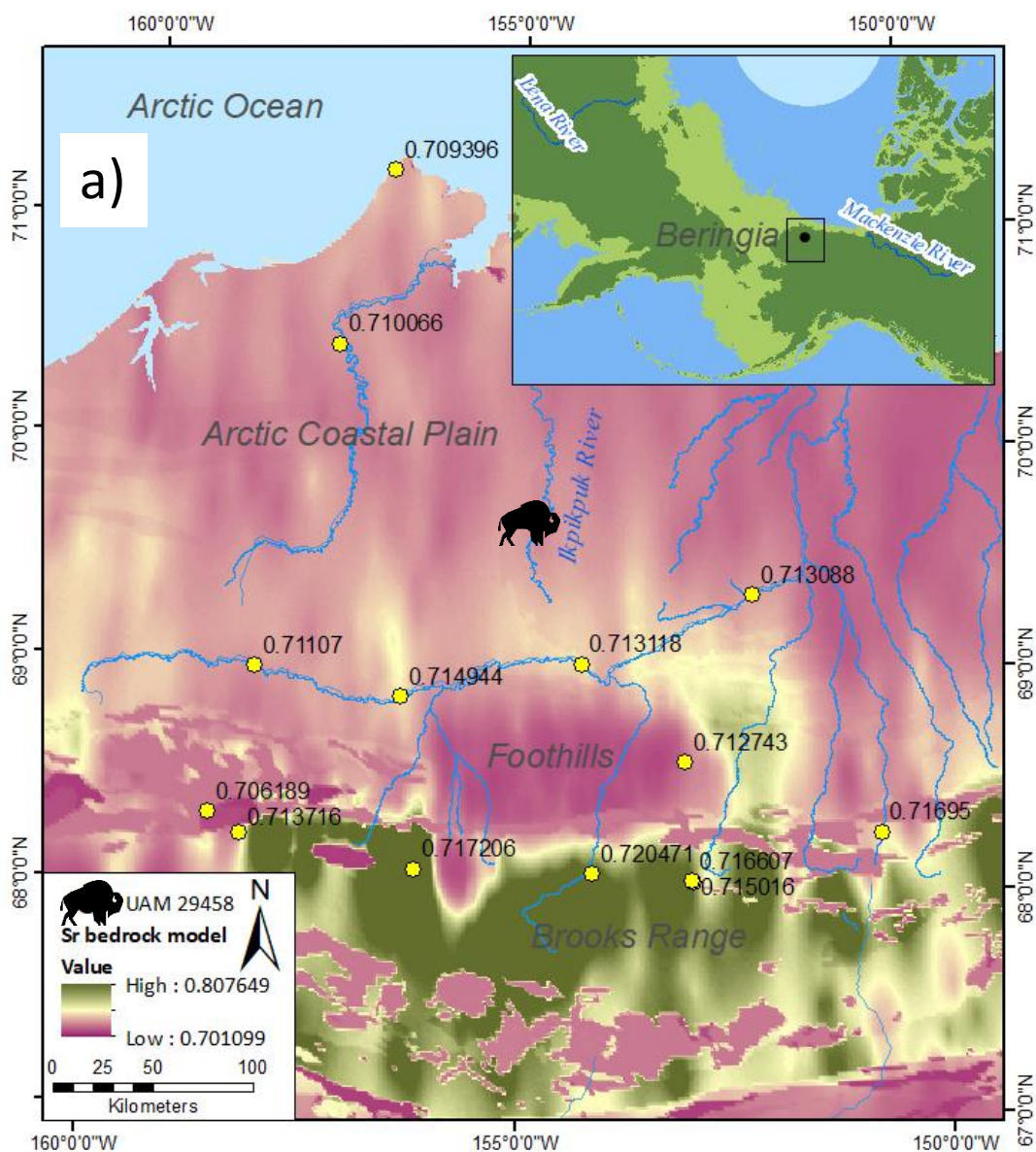


Figure 2

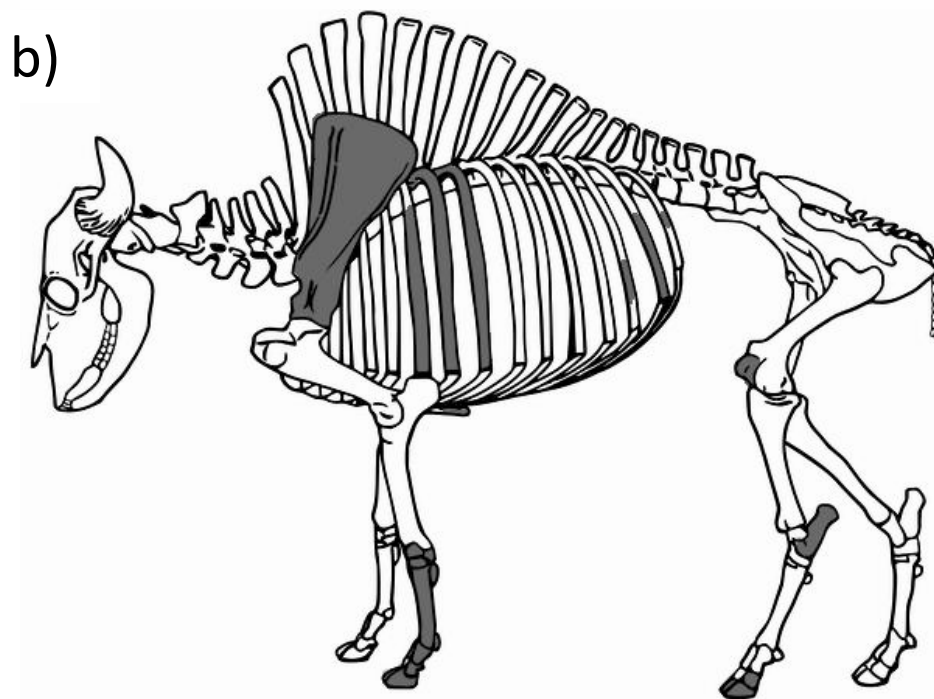
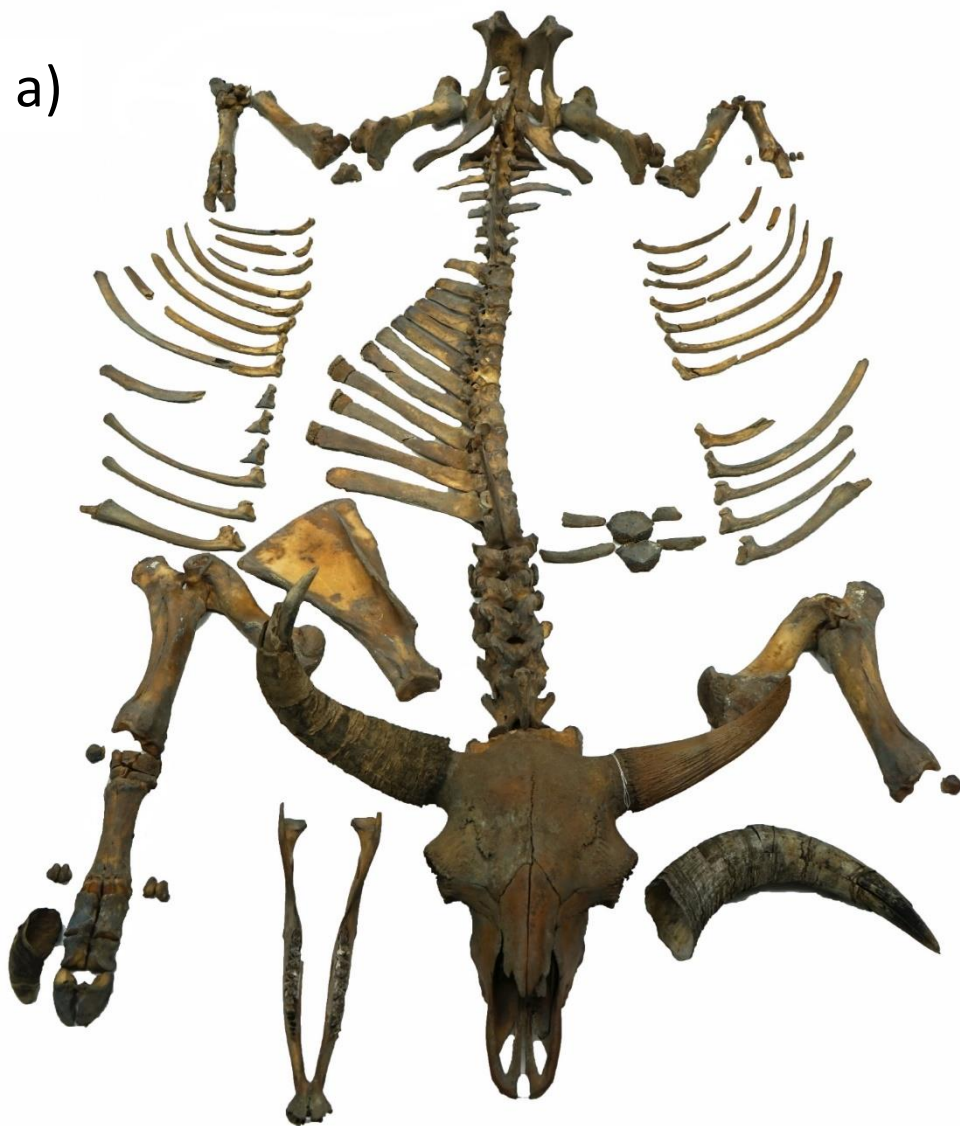


Figure 3

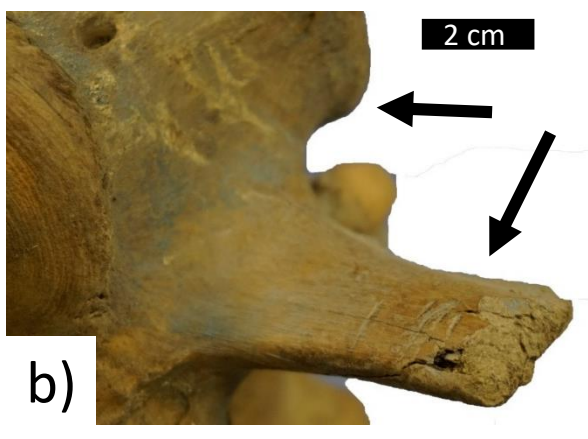


Figure 4

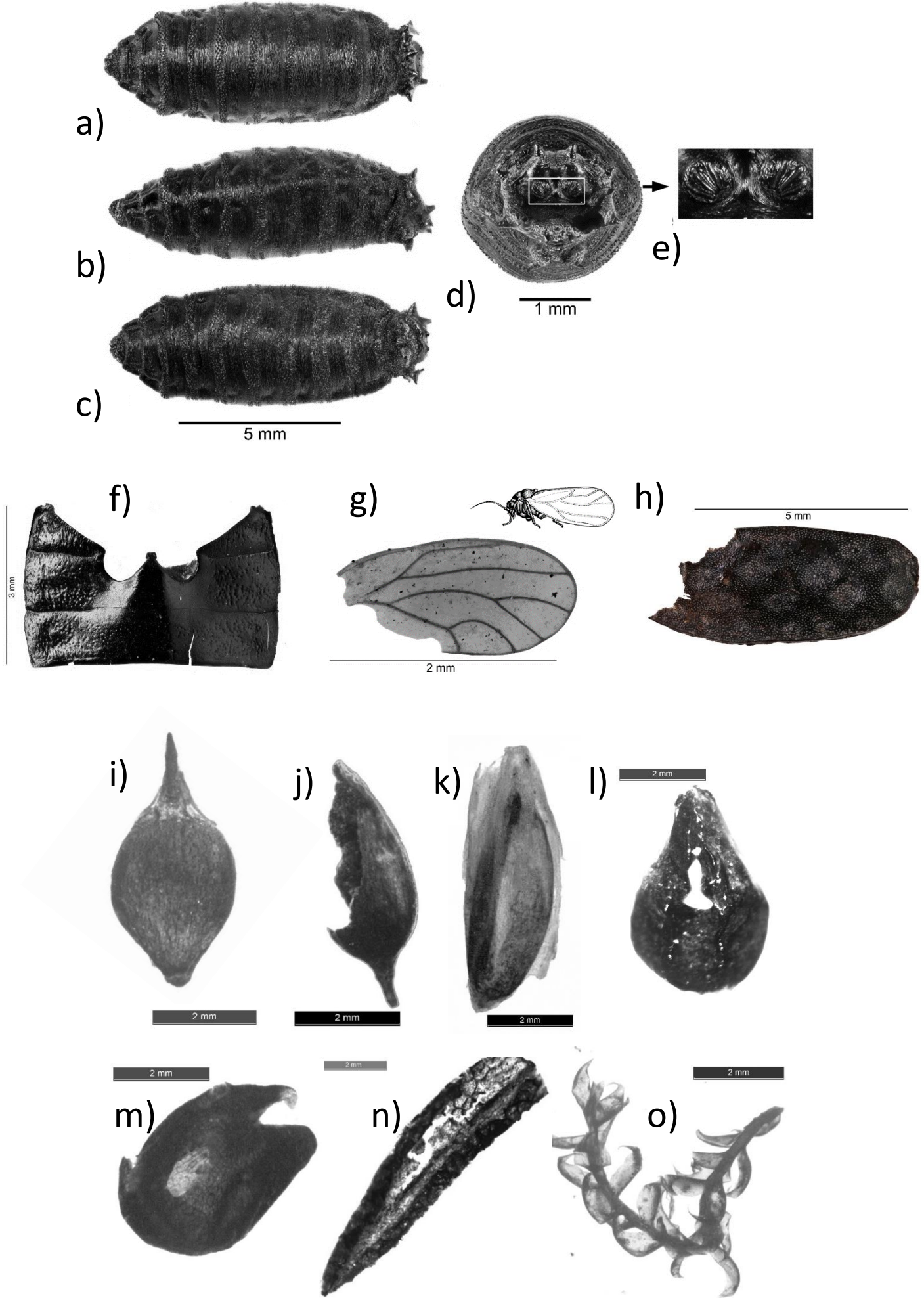


Figure 5

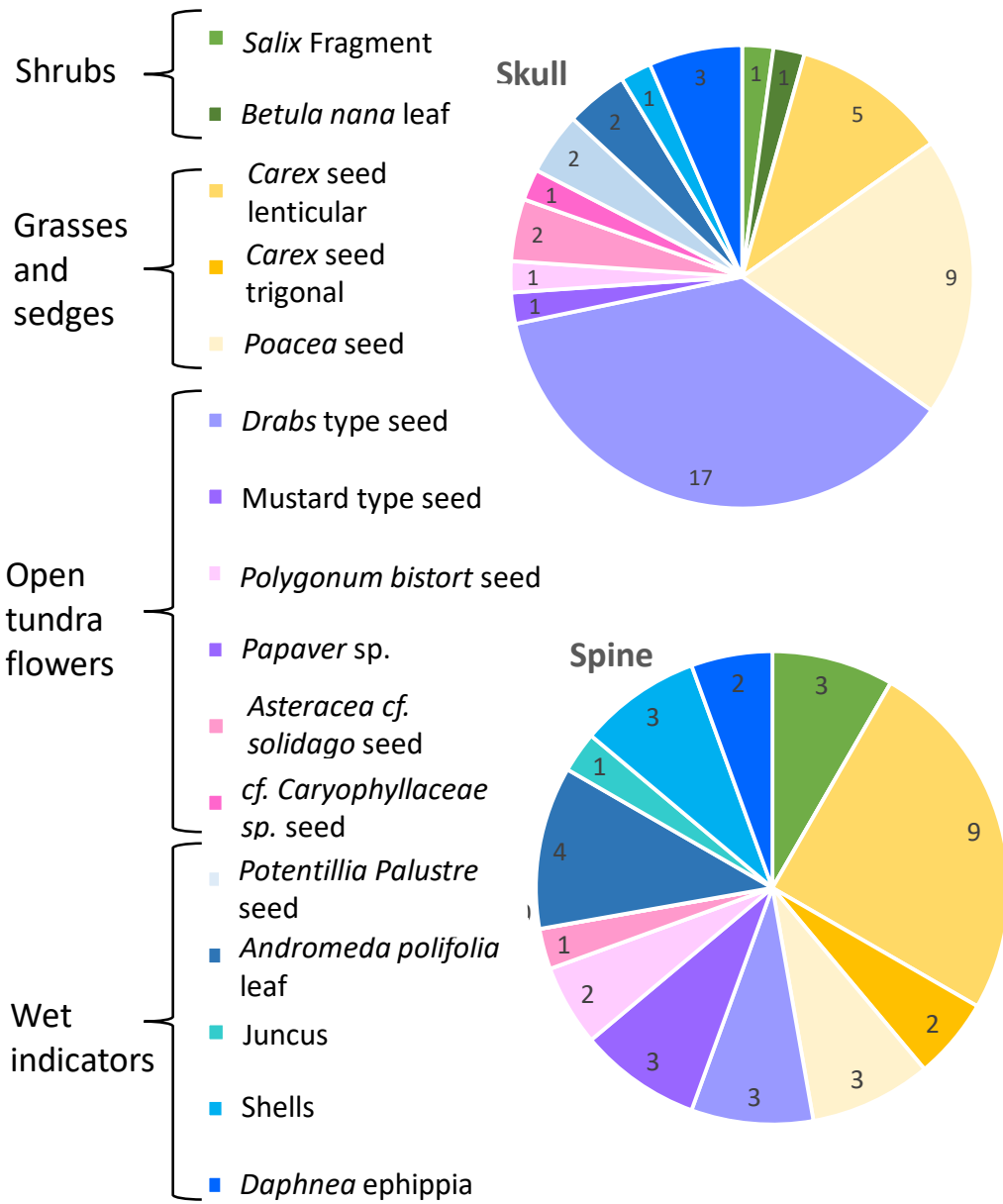


Figure 6

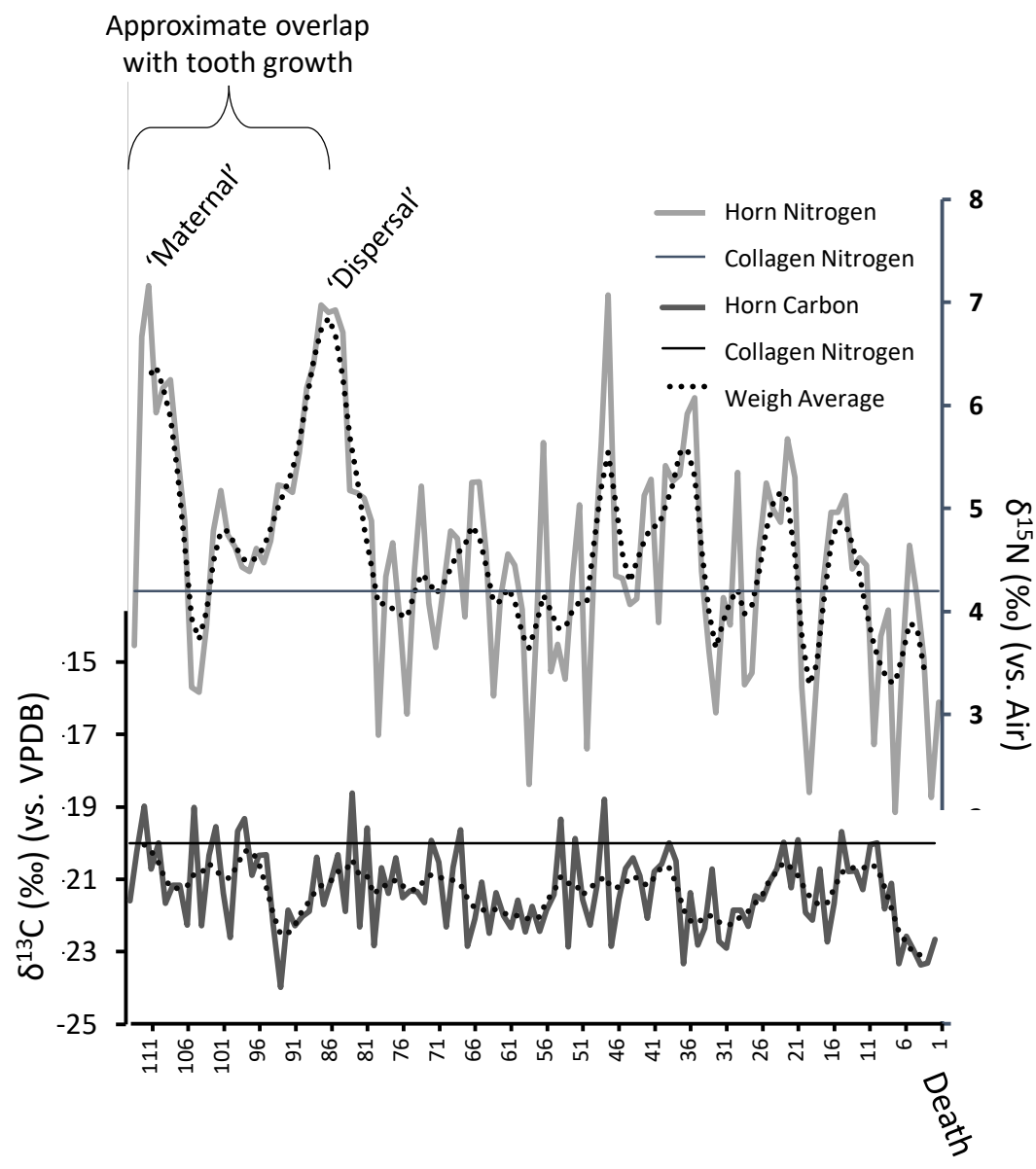


Figure 7

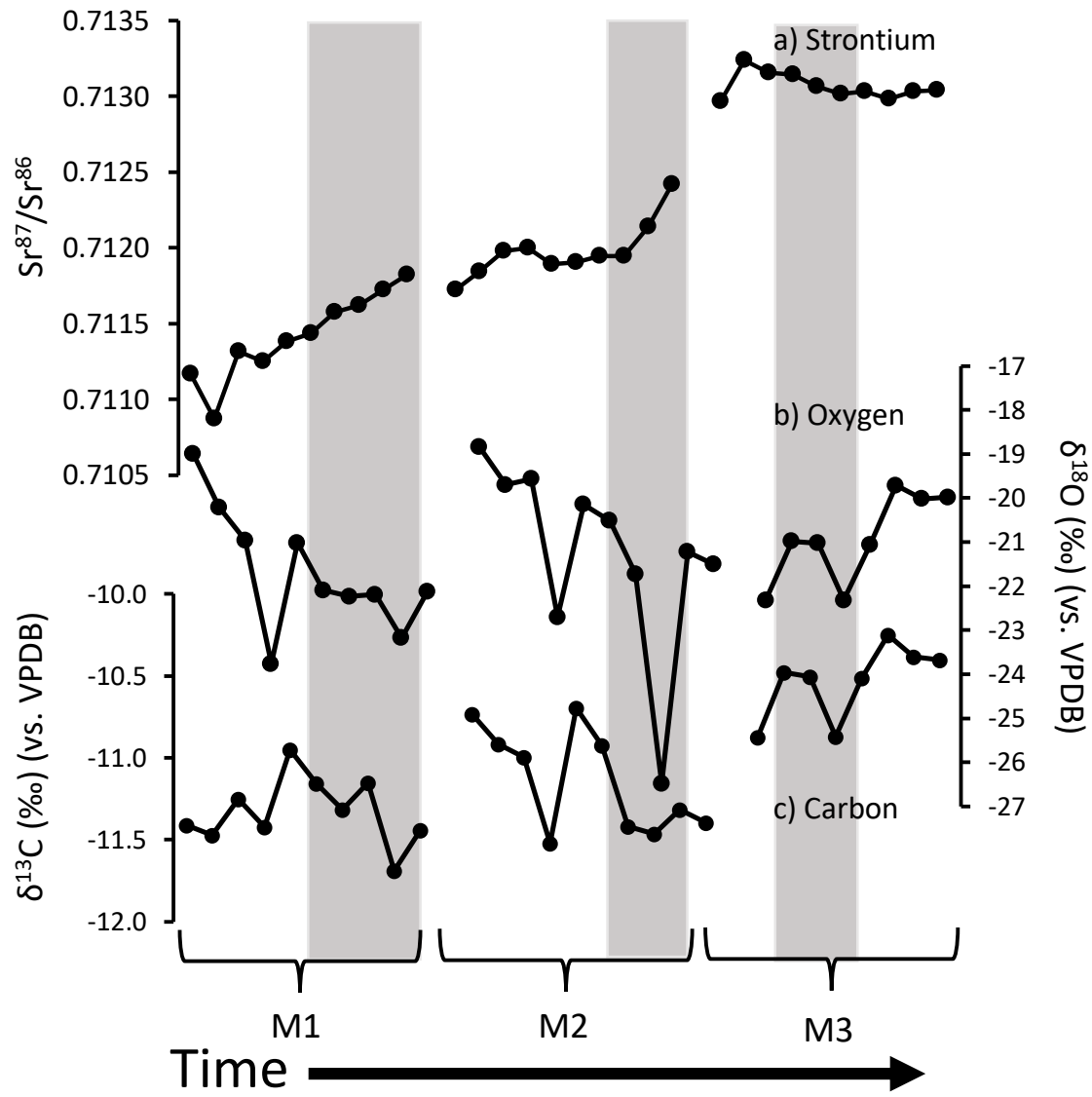


Figure 8

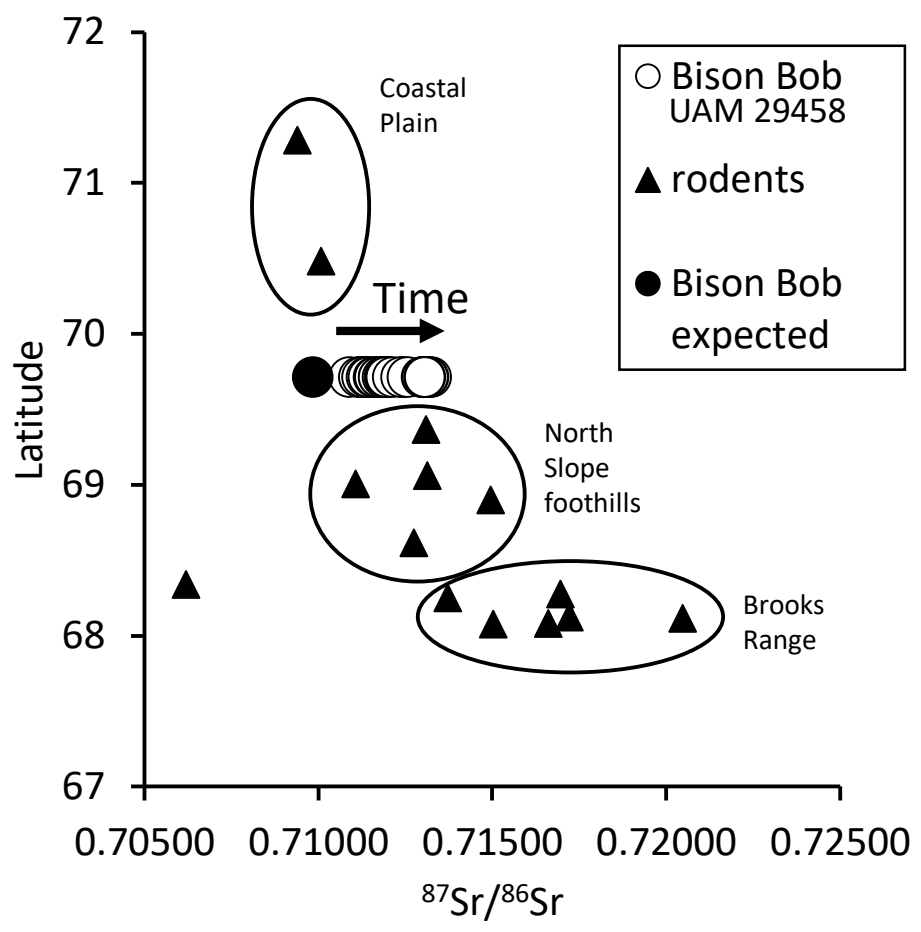


Figure 9

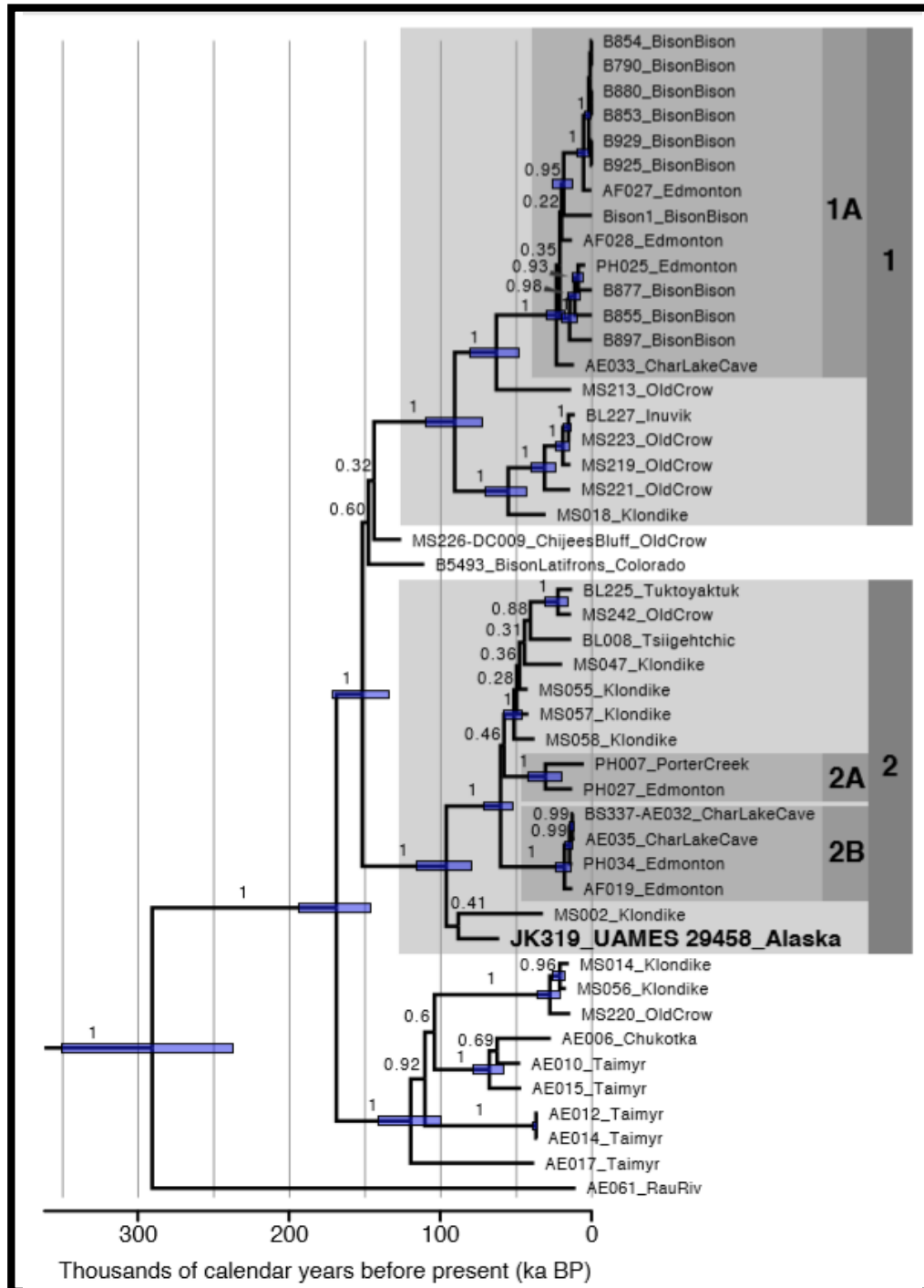


Figure 10

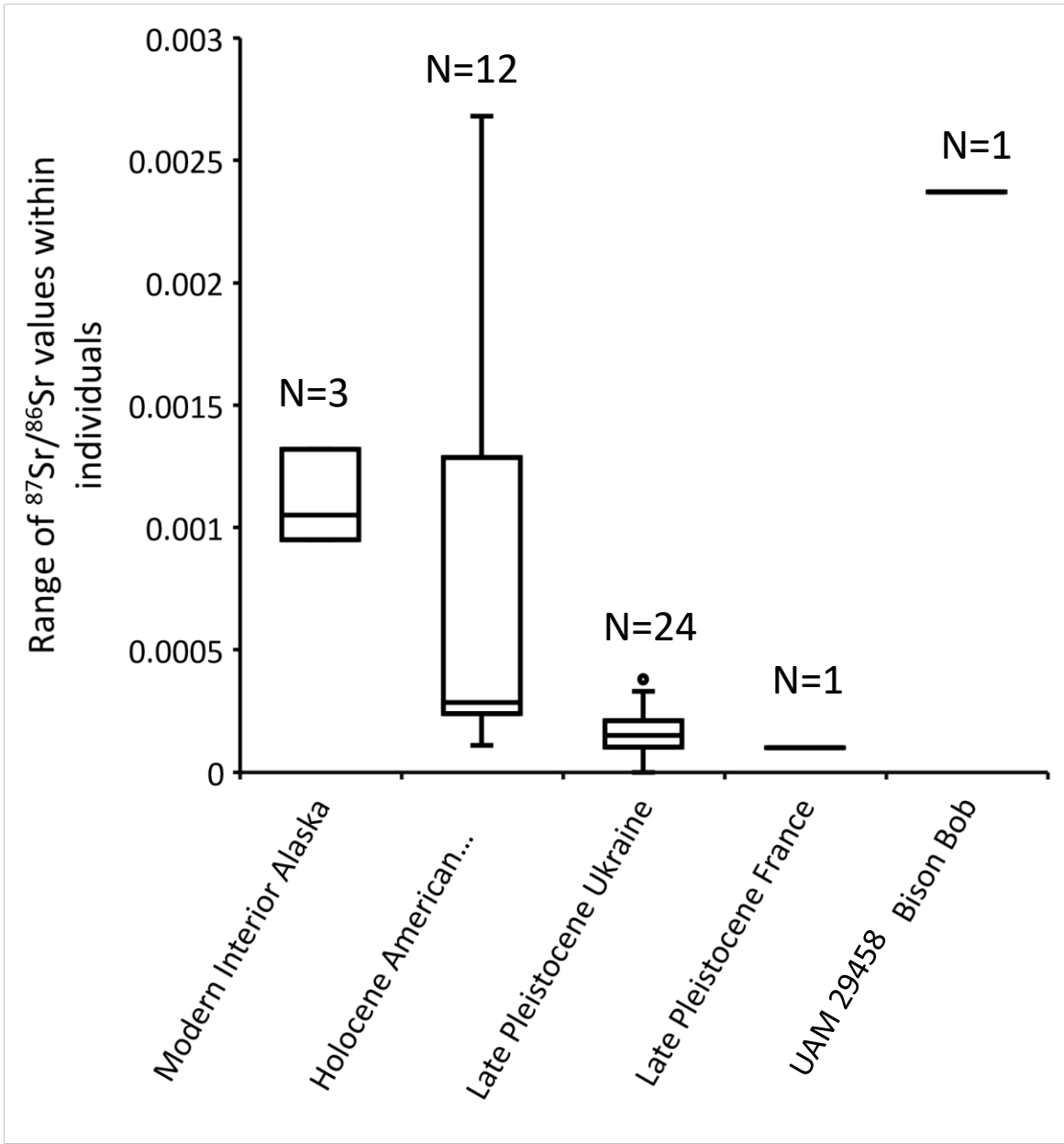
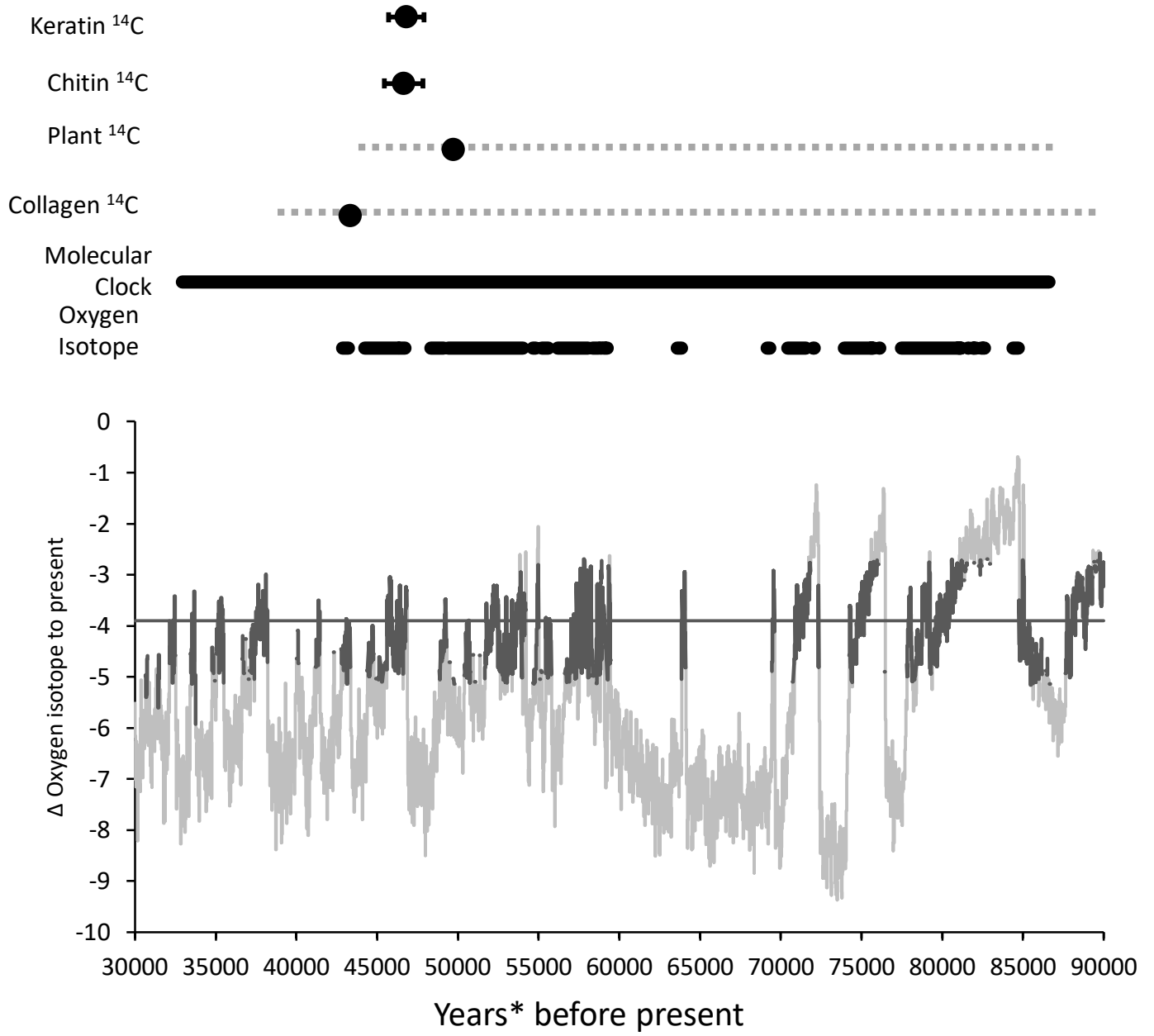
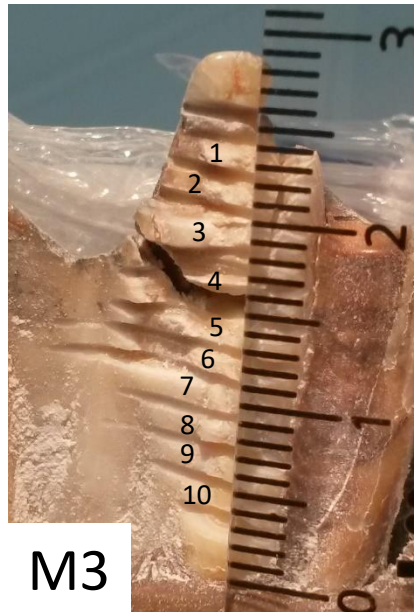
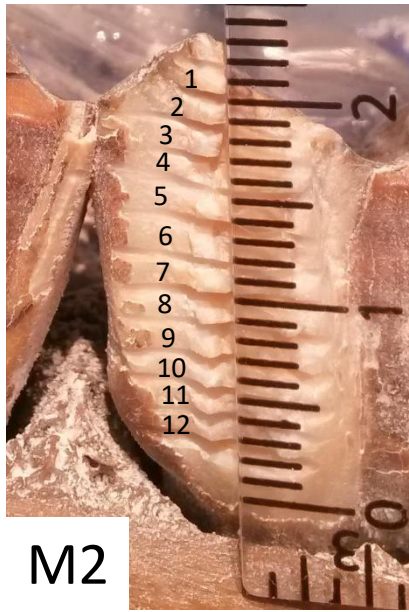


Figure 11



Supplemental materials

S1



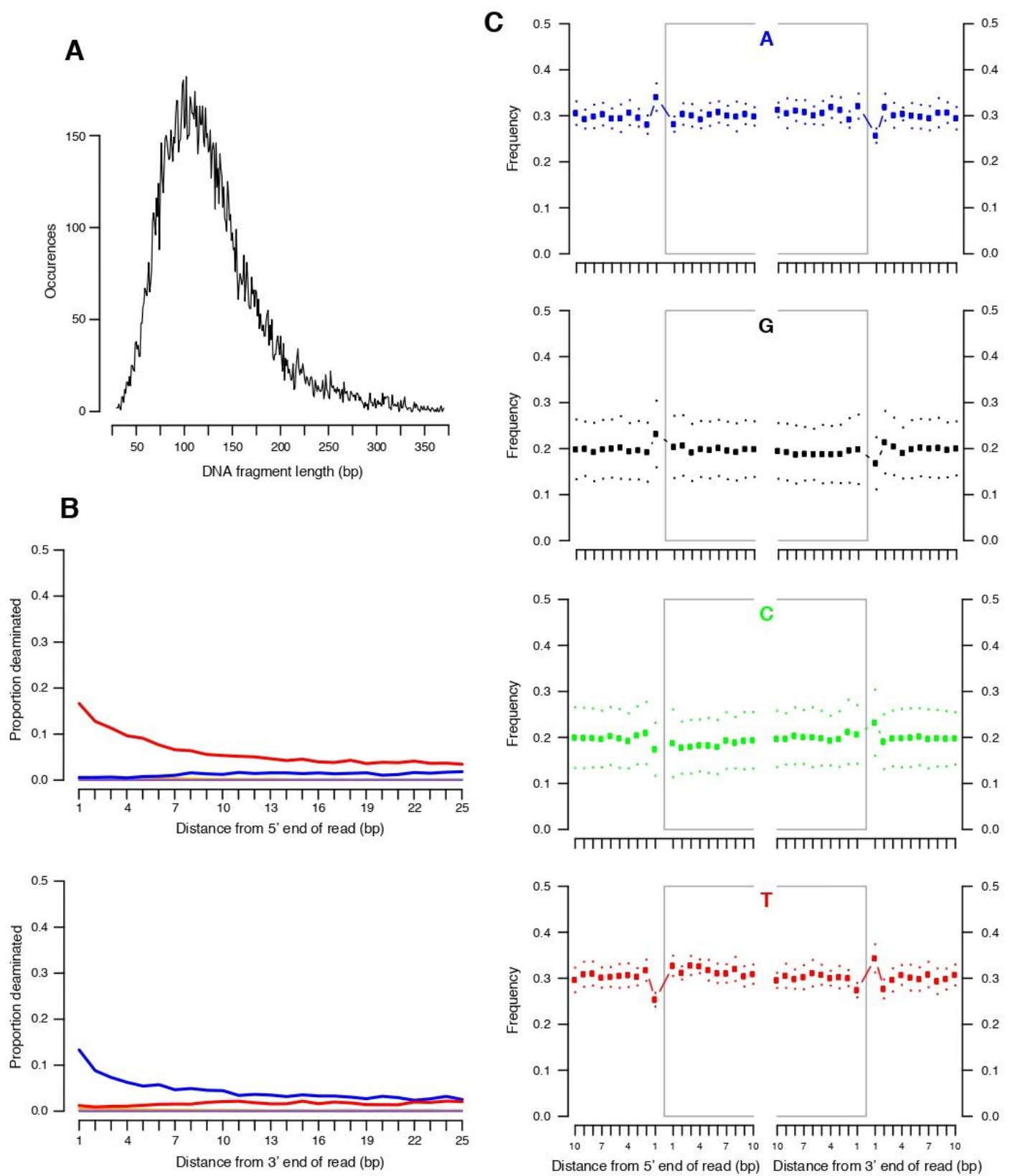
Supplemental materials

S2



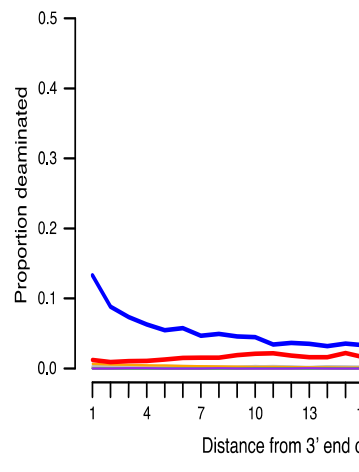
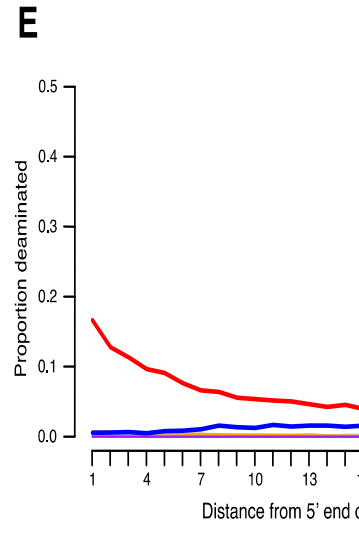
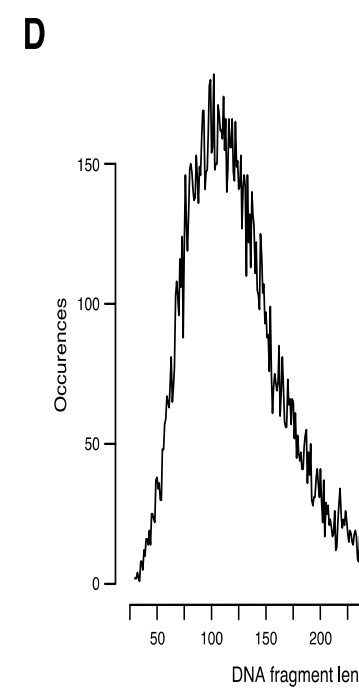
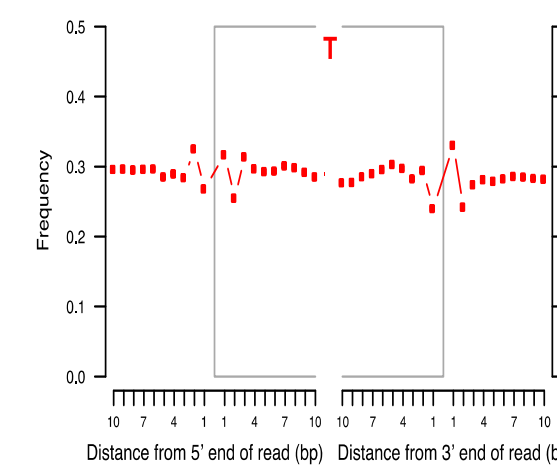
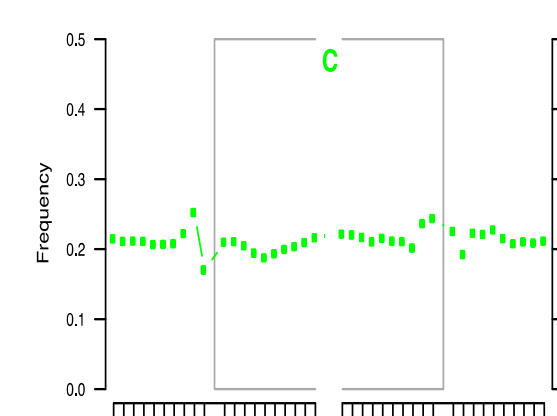
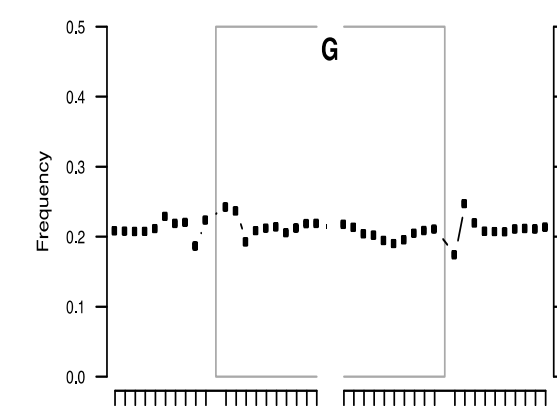
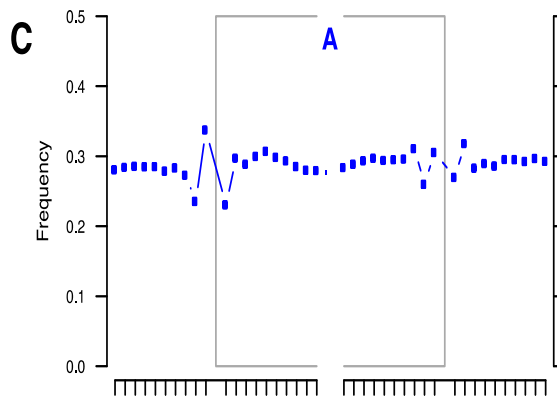
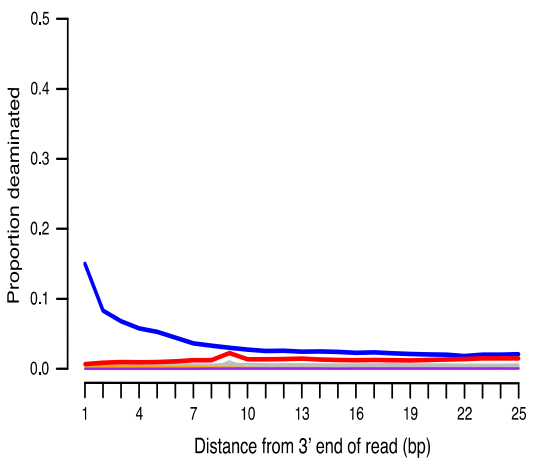
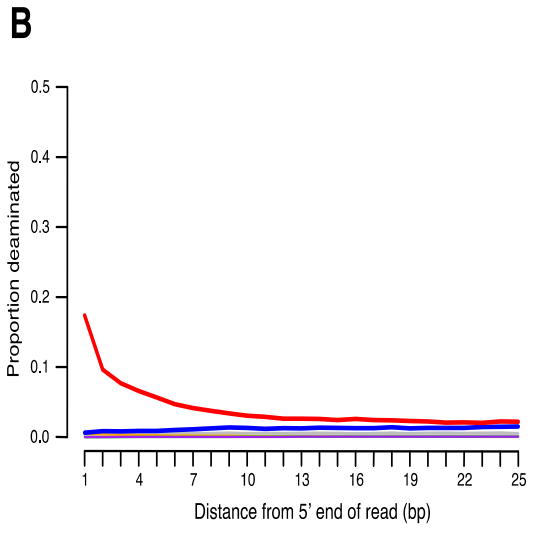
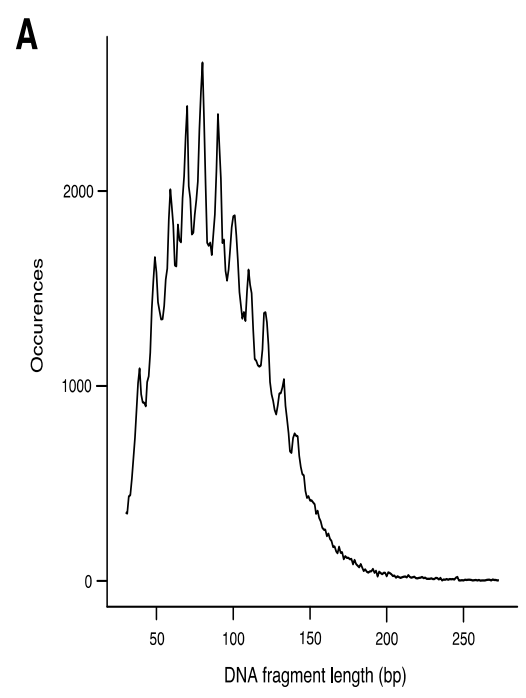
Supplemental materials

S3



Supplemental materials

S4



Supplemental materials

S4

